Assessing the feasibility of using InSAR to improve Landslide Susceptibility Modeling

by

Luca Arbuatti

to obtain the degree of Master of Science in Environmental Engineering
at the Delft University of Technology,
to be defended publicly on Monday March 30th, 2026, at 10:00 AM
in Lecture Hall B at the Civil Engineering and Geosciences faculty.

Student number: 5842921

Thesis committee:	Prof. dr. T. Bogaard,	TU Delft, main supervisor
	Prof. dr. ir. R. Hanssen,	TU Delft
	Dr. ir. A. Urgilez,	SkyGeo

TU Delft SkyGeo

Abstract

Landslide susceptibility modeling is widely used to support spatial planning and risk mitigation, but its reliability is strongly dependent on the completeness and quality of landslide inventories. In recent years, Interferometric Synthetic Aperture Radar (InSAR) has been proposed as a tool to augment these inventories by detecting surface deformation associated with slope instability. However, the conditions under which InSAR-derived deformation can be effectively integrated into susceptibility modeling remain unclear.

This study investigates the feasibility and limitations of incorporating InSAR-derived surface deformation time series into landslide susceptibility modeling for the island of Ischia (Italy), a geomorphologically complex and landslide-prone environment. A traditional susceptibility model was first developed using established static controlling factors, including slope, lithology, soil thickness, terrain wetness index, land use, curvature, aspect, and rainfall. The model achieved satisfactory performance and identified slope as the dominant controlling factor, consistent with the expected behaviour of rainfall-induced landslides.

To assess the contribution of InSAR, deformation time series derived from Sentinel-1 data (2019–2025) were used to generate additional landslide samples based on a statistically defined detectability power threshold. These samples were then incorporated into the landslide inventory to produce an augmented susceptibility model. The analysis focused on comparing three scenarios: a traditional model, an InSAR-augmented model using slope-filtered deformation points, and an augmented model including all InSAR-derived points without additional geomorphological filtering.

The results show that the integration of InSAR-derived landslides does not automatically improve model performance. When slope-based filtering is applied, the augmented model preserves the geomorphological consistency of the traditional model, with slope remaining the dominant controlling factor. However, when InSAR-derived points from low-slope areas are included, model performance decreases and land cover becomes the dominant predictor, indicating that the model is capturing non-landslide-related deformation processes associated with urban areas and observation bias.

These findings demonstrate that standard InSAR quality filtering is not sufficient to ensure that detected deformation corresponds to slope instability. The successful integration of InSAR into landslide susceptibility modeling requires the application of explicit geomorphological constraints, particularly slope-based filtering, to exclude deformation signals unrelated to landslide processes. InSAR should therefore be considered a complementary data source whose value depends on careful filtering and interpretation, rather than a direct replacement for traditional landslide inventories.

Contents

List of Figures

List of Tables

1 Introduction

1.1. Background

The term ”landslide” comprehends the movement, failure or fall of a certain parcel of slope, regardless of whether it acts on loose or rocky material. Such movements can be caused by seismic, hydro-meteorological and human activities, and can variate in size from small rock falls to hundreds of km-square of parcels. Depending on their size, speed and frequency, landslides can have a significant impact on human society and the surrounding environment.

Researchers over the years have shown how the impact of landslides can broadly span between low economic costs to fatalities. While the recording of landslides traces back to decades, first in a paper-based and subsequently in a digital way (Emberson et al., 2022), the collection and archive of the consequences of such landslides is still rare. Several studies have been conducted on both regional (Sepúlveda and Petley, 2015; Haque et al., 2016; Haque et al., 2019) and global scales to estimate the impact that landslides have on fatalities (Fidan et al., 2024; Emberson et al., 2022; Petley, 2012). It has been estimated that about 56000 people have been killed by 4862 landslide events between 2004 and 2016, with a heterogeneous distribution across the globe (Froude and Petley, 2018). Several ”hot spots” can still be identified, such as the Andean region in South America, China and South-East Asia, Eastern Africa and the Alps in Europe (Froude and Petley, 2018; Kirschbaum et al., 2015). When zooming in on a national or regional scale, it appears how even more developed countries are not exempt from casualties due to landslides. For instance, between 1920 and 1999 in Italy only two years (1944 and 1995) have been recorded as free from landslide-induced deaths, with an average of 26 yearly life losses in the last decade of the past century (Guzzetti, 2000).

Besides the well-acknowledged impacts on society, landslides have relevant impacts on different spheres of the surrounding environment as well. The most common impacts are seen as forest destruction (Geertsema et al., 2008) and river flow path disruption or relocation (Schuster and Highland, 2007; Schuster and Highland, n.d.; Korup, 2005). However, it has been seen how the impact goes beyond the direct physical effects that a landslide can have over the landscape: a fact that was understated until the early 2000s is the impact that landslides have on the local ecology and biodiversity. The burial of existing forests or grassland can cause reduction or partial extinction of local micro biota, as well as uninhabitability for the local fauna (Li et al., 2022; Geertsema and Pojar, 2006).

1.2. Problem definition

To date, the two main ways to reduce to the minimum the impact of landslides on societal activities are physical remediation of an unstable slope and land use planning decisions. The former can include the increase of vegetation with non-shallow roots or the use of civil engineering solutions including bolts and meshes (Lazarte et al., 2015; Maddalwar et al., 2024; Stokes et al., 2008), while the latter boils down to assessing which areas are at risk of being affected by landslide (both actively and passively), and making efforts to keep relevant infrastructures elsewhere. Considering the technical challenges associated with it, physical remediation of landslides is rare due to the fact that it is quite impractical

and might lead to high costs.

On the other hand, land use planning can assist in mitigating this potential risk from the root, by leaving areas which have a high chance to be affected by landslides uninhabited where possible, especially when looking at assigning a new anthropogenic use to a parcel of land due to population growth. The assessment of whether an area is prone or not to being affected by a landslide is called a Landslide Susceptibility Assessment (LSA), and it is achieved by making a Landslide Susceptibility Model (LSM), which generates a Landslide Susceptibility Map. It should be noted that this type of assessment is purely based on spatial factors, not including the temporal ones in its assessment (Chacón et al., 2006). A LSA is based on the use of landslide inventories, which generally comprehend date, location and type of mass of a landslide (Guzzetti, 2000; Guzzetti et al., 2012; J., 1984), and maps containing the possible geomorphological and hydrological factors that can be drivers of slope instability. The fundamental principle of landslide susceptibility modeling (LSM) is to quantify the potentially non-linear relationships between observed landslide occurrences and the geomorphological attributes of the corresponding terrain units (Devkota et al., 2012; Lombardo and Mai, 2018; Reichenbach et al., 2018).

Since the 1990s, the development and improvement of Geographical Information Systems (GIS) led to the possibility of modelling or computing the LSA of a certain area on a larger scale, which was seldom done through surveying or physical modelling (Chacón et al., 2006). To date, GIS-based methodologies are coupled with statistical- and Machine Learning (ML)-based models to shed light on the importance of the factors that might control the event of a landslide (Reichenbach et al., 2018). By overlaying all the chosen and available controlling factors for a certain area (slope, aspect, curvature, lithology, land use, rainfall, soil moisture, Terrain Wetness Index; among others) with the landslide inventory, spatial relations are modelled to derive which factors have a relative high or low influence on the landslide location.

This makes the landslide inventory a crucial piece of the modelling puzzle. However, due to the fact that it is in essence a record made by local experts or surveyors and rather than a complete representation of all landslides, several issues may arise (Cascini, 2008; Harp et al., 2011; Steger et al., 2016; Steger et al., 2017). The incompleteness of the inventory itself, which translates to not having all past landslides recorded, was proven to mislead susceptibility relationships between the location of a landslide and its controlling factors (Steger et al., 2017). This incompleteness arises from several factors: the methods used to map the past landslides (Guzzetti et al., 2012); the bias related to the surveyor and the purpose of the survey (Santangelo et al., 2015), the choice on the shape (point, polygon) which then can be converted in a GIS format (Huang et al., 2021).

Given that the goal of a LSM is to find patterns between controlling factors and presence of landslides, the model indirectly searches as well patterns of the factors where landslides did not happen. Typically, the locations not marked as landslides are randomly sampled and used for the model to learn which controlling factors did not lead to a landslide (Guzzetti et al., 2012; Hong et al., 2019; Hussin et al., 2015). This leads to another issue related to the use of landslides inventories: these non-landslide samples (so-called ”0” samples) can reflect any portion of the study area, including moving slopes. This absence of sub-classification within the non-landslide samples can lead the model to learn patterns that do not reflect the real physical processes, and does not account for the movements that are present before failure events. Such a displacement activity prior to failure has been seen to provide valuable insights on the nature of landslides (Intrieri et al., 2017), leaving potential for its inclusion in performing a LSA.

One way to include this displacement is to use it as a tool to determine whether a slope is moving fast enough to be considered unstable, and add the unstable slopes to the landslide inventory. This methodology was firstly explored by Chen et al. (2023), where InSAR was used as a tool to detect slope instability, and areas moving faster than a pre-defined velocity were added as extra landslides to the original inventory. Still more aspects should be tackled, such as the derivation of a displacement threshold for each different study area in a quantitative way. This has been explored further by Feng et al. (2025), where a mixed dataset of InSAR and GNSS displacement was created and the probability density function (PDF) of such displacement velocities was used to determine multiple velocity thresholds. Thereafter, the optimal threshold was chosen in an empirical way as the one with the highest

model performance. This new methodology has proved to show improvements in modelling performance, however it only tackled the uncertainty that is associated with InSAR by using a coherence threshold, which can be misleading in the way how InSAR time series are interpreted.

1.3. Objective and research questions

Based on the above standing narrative, the main research objective of this research is **to improve the feasibility of using the combination of InSAR displacement data and landslide inventories to improve landslide susceptibility modeling by using appropriate InSAR quality parameters**.
This objective is summarized in the research questions presented in the following main research question:

What are the critical success factors for applying InSAR displacement time series in the landslide susceptibility assessment?

To answer this question, the following sub questions are formulated:

1. *Which parameters affect the accuracy and quality of InSAR time series used for LSM?*
2. *How can temporal displacement patterns be used to derive appropriate dynamic controlling factors, such as hydro-meteorological data?*
3. *How can displacement thresholds be implemented as decision boundaries between landslide and non-landslide samples?*

2

Background

This chapter provides the background required for this research. It mostly includes the literature review performed to find existing knowledge, related findings and research gaps regarding the three main topics of this project. Section 2.1 describes landslides types and their physical processes. Section 2.2 provides relevant statistical and ML-based models developed in LSM and their practical use in spatial planning. problems. Section 2.3 focuses on the basics of the InSAR technology and its use for slope movement detection.

2.1. Landslide background

2.1.1. Slope movement mechanics

A widely accepted common definition of landslides is that they are ”the movement of a mass of rock, debris or earth down a slope” (Cruden, 1991). When a slope is unstable, the equilibrium between the shear stress and its shear strength is not present anymore, and the force expressed by gravity overcomes the friction between the soil particles (Bogaard and Greco, 2015).

On a soil pores scale, gravity is the driver of shear stress, while on the shear strength side there are multiple factors playing a role: soil friction, which resembles the physical friction between soil particles that are adjacent to each other; soil suction, which is the phenomenon at which air that is constrained between soil particles keeps these particles ”sucked” together, therefore making soil behave as a whole (Fredlund and Rahardjo, 1993); soil cohesion, which describes the electrochemical bonds between the mineral compounds within the soil (Bogaard and Greco, 2015).

However, the above-mentioned processes do not take yet into account the active role that hydrology has on slope movement. In unsaturated soils, water from rainfall enters the pores between the soil replacing the space occupied by the air, or fills part of this volume, exerting a pressure that reduces soil cohesion, friction and suction (Bogaard and Greco, 2015). This decrease in the shear strength of the soil leads to an imbalance in the original equilibrium of a stable slope, making rainfall one of the main drivers for slope instability (Iverson, 2000). On the other hand, slope instability can be caused also from water entering the soil matrix from underneath it, and not only from above the surface. In fact, rise in groundwater level can also increase pore water pressure, leading to a higher risk of instability.

The most important parameter that drives the movement of water through the soil is the hydraulic conductivity K, which describes the ability of soil of allowing water flow within the soil matrix (Bogaard and Greco, 2015; Iverson, 2000). Generally, soils with a low K tend to have a higher risk of slope instability when affected by rainfall or groundwater level rise, since water that cannot flow through the soil pores tends to accumulate and increase pore water pressure at a higher magnitude (Iverson, 2000).

2.1.2. Landslide types

Classification of landslides is a field that grew during the mid-1900s and many currently accepted terminologies were developed during the 1970s by Varnes (1957). Landslides and soil processes are

classified based on several factors: the type of material that displaces (Varnes, 1957); the depth with respect to the ground level of the displaced material (Hungr et al., 2013); the driving mechanism (Hungr et al., 2013); the type of mechanism that the displaced material follows during the failure (Varnes, 1957). Since this section only serves as background knowledge related to landslides, only certain major classifications and aspects will be covered.

Several types of materials can be classified within a landslide event, however the main 2 categories are materials under the soil type family and the rock type family (Hungr et al., 2013). These two materials generally exhibit different behaviours: while soils show slow and more constant movement when triggered by rainfall or other events, rocky materials tend to have a more sharp type of displacement, which may also be caused by internal stresses within the rocks.

When looking at the movements that slopes can exhibit, these are generally classified by the morphological process behind the instability, and the consequent ”scar” that landslides leave on their path; this kind of classification is generally the mostly used within existing literature (Hungr et al., 2013). Among common landslide types we find falls, which appear when definite portions of rock detach from the main rock body on steep slopes and bounces or falls through the air. Such events are typically preceded by small and sharp accelerations, and free fall is almost certain for slope > 76°(Varnes, 1957). This is a common event in the Yosemite National park in the USA, where >850 rockfalls have been recorded since 1857 (Stock et al., 2011).

Another relevant type of instability is toppling, which happens when a certain portion of a slope pivots over a point lower in the slope, and the barycenter of a certain mass of the slope ends beyond the slope itself. This can be caused by internal stresses or geological features in a slope, or by the pressure exerted by the fluids within the rock, both at the liquid of gaseous state (Varnes, 1957). A typical example of this type of movement is the failure close to the Tonco valley in Argentina in dating back to 15000 years ago studied by Evans et al. (2006).

On the other hand, slides comprehend the rotational or translational movement of a certain parcel of land which can be progressive over time, and can extend its footprint from the initial affected area (Varnes, 1957). A clear and recent example of this is the Niscemi landslide in Sicily (Italy) from January 2026, where a combination of translational and rotational failures have led to a ˜15m of displacement (Protection, 2026). Moreover, another relevant landslide type are flows, which appear when high displacement velocities make the rocky or loose material behave like a liquid, in most cases happening where water is present Varnes, 1957). A clear example of such type of landslide is the debris flow happened on the island of Ischia (Italy) on November 26th, 2022, leading to two casualties (Danesi et al., 2025).

2.2. Landslide susceptibility modeling

2.2.1. Landslide susceptibility modeling in spatial planning

In general terms, a LS assessment is used in many aspect and at many scales during spatial planning. These can vary from its use for the development of a neighborhood, to a regional scale to assess safety in national parks or to build nation-wide infrastructure such as highways or railways (Fell et al., 2008). To highlight the relevance of the efforts that have been given to this field since the 1970s, it is important to highlight more examples of when landslide susceptibility assessments are important:

- Residential land development, such as the creation of new neighborhoods or the allocation of rural land plots
- Decision making in allocation of society-relevant infrastructure, such as hospitals, airports, educational or jurisdictional institution
- Major supply lines, such as (waste)water and gas pipes, or electricity lines
- Communication lines such as roads, highways, railways, including both above- and underground infrastructure such as tunnels

- River valleys where dams are planned to be constructed, to avoid catastrophes such as the Vajont dam in 1963 where 2000 people lost their life (Kilburn and Petley, 2003)
- Allocation of recreational activities, such as mountain trails, management of rocky coasts and state forests

However, the active use of LS map is not always present in land-use planning. This is because there can be a mismatch between the scientific scope of creating a LS map and the practical use of it from the local authorities, due to the usability that these maps offer (Bell et al., 2013). For instance, it has been seen how susceptibility models require several local data, which sometimes it is not possible to be provided from the local authorities (Bell et al., 2013; Van Westen et al., 2008); this is often the case especially in developing countries (Nugraha et al., 2026). Another important fact is that distinctive maps made from the same contextual data but with different models appear to have a different susceptibility class in certain areas, which makes authorities reluctant to trust the susceptibility results (Huang et al., 2024). Furthermore, the limitation of the available data and especially of the landslide inventory can lead to high uncertainty of the model results, especially in the areas not covered by the landslide inventory (Huang et al., 2024; Woodard and Mirus, 2025).

2.2.2. Landslide susceptibility modeling background

As stated in section 1.2, the goal of a LS model is to learn the non-linear patterns between the controlling factors and the landslide inventory, and translate that into a susceptibility probability for each portion of the AOI. Initially, this was done in a ”qualitative” way, where the degree of susceptibility was expressed in descriptive terms rather than quantitative probabilities (Reichenbach et al., 2018; Van Westen et al., 2008). Such qualitative assessments heavily relied on the expert's knowledge of the area, and their skills in understanding or assuming the relevant controlling factors.

It appears clearly how such approaches could lead to a wrong estimation of the landslide's controlling factor, therefore quantitative methods were developed as well. Initially, physics-based methods were used, where hydrological data was coupled with soil properties parameters and soil thickness to derive the movement of shallow landslides (Montgomery and Dietrich, 1994). In general terms, the most widely-used physical models for landslide susceptibility rely on the fundamental principle of slope hydrology (Montgomery and Dietrich, 1994; Rigon et al., 2006).

Besides physical models, the most used LS models are statistical models (Reichenbach et al., 2018). As mentioned in Section 1.2, these models rely on the assumption that landslides appear in areas with similar controlling factors, therefore it is possible to exploit the inventory of past landslides to extrapolate where highly susceptible areas might be on slopes with no recorded landslides. The main classification methods found in the existing literature are: linear and logistic regressions, discriminant analysis, index-based weight-of-evidence (WoE), machine learning, neural networks, and multi-criteria decision analysis (Reichenbach et al., 2018).

A pioneering work by Carrara (1983) showed how the use of multivariate models could be exploited to derive one of the firsts data-driven LS map. In his work for each terrain unit several controlling factors and the landslide inventory are listed, and a linear equation is used to derive the (in)stability of such a terrain unit:

$$D = a_1x_1 + a_2x_2 + a_3x_3 + ... + a_nx_n \tag{2.1}$$

where x are all the controlling factors, a the statistically-derived weights for each factor, and D the (in)stability discriminant, where $D > 0$ reflects unstable areas, and $D > 0$ represents stable areas.
By dividing the discriminant factor D in two classes (stable and unstable), the computation of the weights is conducted in such a way to **maximize** the separation *between* the two classes across all the units, and to contemporarily **minimize** the *within* class variance. However, the limitations of such model should be mentioned as well: the assumptions of linear relationships between the controlling factors and the landslide appearance and the independence of the controlling factors were still not treated at the time. Furthermore, model validation and testing were still not applied.

Other commonly-used models are probabilistic prediction models, which use the spatial distribution

of past landslides to compute the probability of whether a landslide will happen at a certain location (Chung and Fabbri, 1999). This type of model calculates the probability of landslide occurrence for each class of every controlling factor by using joint conditional probability:

$$P(L|F_1, F_2, F_3, ..., F_n) \tag{2.2}$$

where L stands for landslide occurrence, and F is each controlling factor. An important advancement of this model was the introduction of a training and validation set within the data. On the other hand, an important downfall on the use of such models appeared to be the class delineation within each controlling factor, as continuous factors such as slope, elevation and any elevation-derived factor require a subjective delineation of the between-class boundaries.

Among statistical models, logistic regression is possibly the most common (Lombardo and Mai, 2018; Reichenbach et al., 2018). The outcome of such a model is still a probability of whether a location would have a landslide or not, therefore following the approach of Chung and Fabbri (1999). However, the way it is achieved is very different: while Chung and Fabbri (1999) use classes for controlling factors and apply joint conditional probability, Lombardo and Mai (2018) uses the following equation to derive the landslide probability:

$$P(L = 1 \mid X) = \frac{1}{1 + e^{-(\beta_0 + \beta_1 x_1 + \beta_2 x_2 + \cdots + \beta_n x_n)}} \tag{2.3}$$

where L stands for landslide occurrence, X stands for the combination of the controlling factors, x is each controlling factor, β_0 is the intercept, and β_i are the regression coefficients estimated from the data, which represent the log-odds change of landslide occurrence.
Another important contribution by the work of Lombardo and Mai (2018) is focusing on the importance of having a balanced training dataset, which was not common practice before. By balancing with a $1:1$ ratio landslide (”1”) and non-landslide (”0”) samples, there is avoidance of encountering biased regression. This is because when having hypothetically 100 ”1” samples and 100000 ”0” samples over the whole AOI, the model would only learn to predict everything as a non-landslide given the very low occurrence of landslides.

Machine Learning for Landslide susceptibility modeling
All the above-mentioned statistical models have common limitations: assuming linear relationships between controlling factors and their weights and not capturing non-linear terrain interactions have been a common challenge. Therefore, the recent rise of ML models has seen the adoption of such approaches also in LS. Different types of ML models have been applied to LS modeling, with the most common being: random forest, support-vector machine, neural networks, gradient boosting, naive Bayes. Given the choice of using random forest (RF) and extreme gradient boosting (XGB) for this research and that investigating each model’s performance is not the main goal of this study, only these two models will be shortly discussed below.

RF is a supervised algorithm laying its foundations on decision trees, where each tree fits an independently sampled subset and is added to the decision workflow of the model (Ado et al., 2022; Merghadi et al., 2020). As trees are added to the forest, variable importance and internal unbiased errors are stored within the model to lead towards the best decision on each subsequent split. The randomness in RF aids to reduce overfitting by splitting nodes on the best tree on each random subset and by building sets of parallel and deep trees. Important hyperparameters to tweak in such models are the maximum number of trees, and the maximum depth of each tree (Merghadi et al., 2020). Since their early implementation in LS in 2010, they have been proven to achieve >90% accuracy in a study conducted by Dou et al. (2019).

XGB is also structured on decision trees, however each new tree here is not used to randomly subset data as RF, rather to correct the ”mistakes” of the previous trees. XGB includes L1 and L2 regularization in the loss function to prevent overfitting and to incentivize the use of simple models over complex ones (Agboola et al., 2024). This gives a penalty which is used in over-complexity mitigation and aids in following the goal of minimizing the loss function between the expected and predicted values.

2.3. InSAR for slope movement detection

After the first successful attempt to measure displacement's over the earth surface, Interferometric Synthetic Aperture Radar (InSAR) became a world-spread technology (Massonnet et al., 1993). In a nutshell, InSAR is satellite-based remote sensing technique based on the core principle of estimating the phase difference between two SAR acquisitions captured at a different moment in time, allowing the user to estimate displacement at the mm precision (Hanssen, 2001; Massonnet et al., 1993). To date, the two most common processing approaches are: Persistent Scatterer Interferometry, where the phase information of stable scatterers (buildings, rock outcrops) are used to reduce atmospheric and decorrelation components in the signal and achieve a higher precision (Ferretti et al., 2001); Small Baseline Subset (SBAS), which exploits whole interferograms with a small temporal and spatial baseline of the image pairs to reduce atmospheric noise and increase displacement estimation accuracy.

When estimating slope displacements, the InSAR technique offers the advantage of having approximately global coverage and have a holistic view on the AOI. This gives the advantage of saving costs and time when compares with in-situ monitoring techniques such as leveling, GNSS, prisms or ground-based radars, since these require site intervention of placing sensors and the maintenance of these. Furthermore, InSAR allows the user to have potentially full coverage over the AOI, which can provide insightful information of whether different parts of a slope are moving in a different way relative to each other.

In the landslide research field, InSAR has been used for several purposes: the main objective is to conduct historical analyses or real-time monitoring of past or ongoing landslides (Vinueza et al., 2022; Kang et al., 2021); attempts have been made in using InSAR to predict slope movement (Li et al., 2022); and applications have been tested in LS modeling as well (Feng et al., 2025; Wei et al., 2024; Zhu et al., 2022).

2.4. Study Area

The selection of a suitable location for this research is defined by several specific criteria: possibility of monitoring displacement with InSAR, presence of displacement patterns, and availability of a landslide inventory. Based on these criteria, a suitable location was found as the island of Ischia, circa 15 km offshore the Gulf of Naples, Italy. The island has a surface of $46.3\ \mathrm{km2}$, and has roughly 62000 inhabitants. The main carried activities are tourism, fishery and agriculture. Almost 50% of the total area is urbanized, while approximately a quarter of it is dedicated to forest use, with the remaining parts dedicated to agricultural and non-economical uses (Appendix A). The high presence of urbanized areas makes it a suitable location for InSAR monitoring on the island.

2.4.1. Topography & Climatic features

The island has a typical volcanic cone shape, with the highest point having an elevation of 784 m and located in the central-western part of the island. Four weather stations are located on the island, respectively in the towns of Ischia, Forio and Serrara Fontana, while the fourth is placed near the summit of the Mount Epomeo (Figure 2.1).

In the past 20 years the island has received on average $840mm$ +/- $70mm$ of annual rainfall, with the summer being the warmest and driest period, and rainfall events mainly happening from October until April. Landslides, however, are typically triggered by intense and extreme events, therefore Intensity-Duration-Frequency (IDF) curves were generated from rainfall data across the four stations, and the average was computed for the whole site. Since rainfall data was available only for the past 18 years, only IDF curves up until a 25-year return period were generated to avoid extreme extrapolation. Figure 2.2 shows the computed IDF curves, which highlight the short rainfall duration regime of the island, which is typical of Mediterranean areas. Furthermore, the uncertainty bands show a higher spatial variability among the stations for short rainfall durations, and lower variability for longer events. This highlights the fact that high intensity, short events are very localized, as longer and lower intensity events are more spread over the entire island.

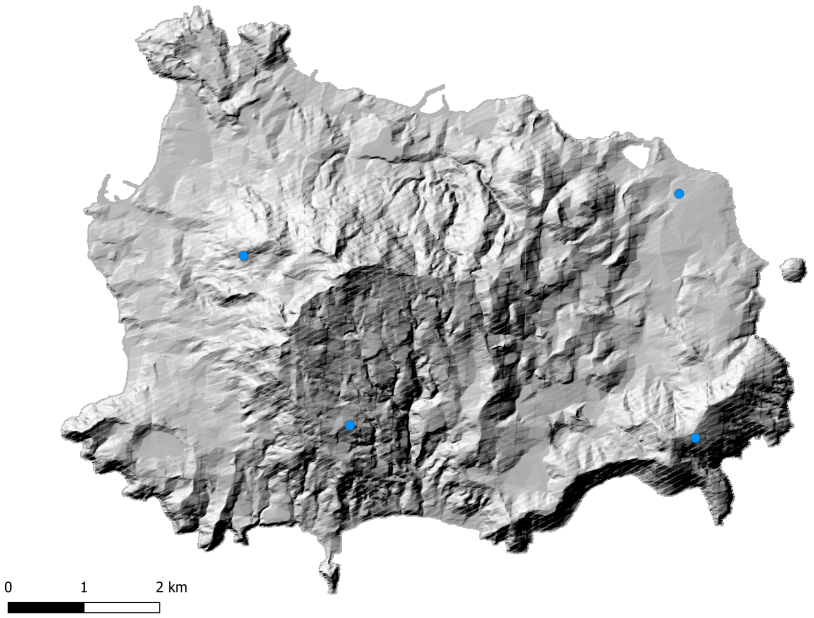

Figure 2.1: Hillshade map of the island with rainfall stations highlighted in blue

2.4.2. Lithological and geological background

A map of the main lithological compositions of the island is shown in Appendix A. The island is part of the Phlegrean Volcanic District (PVD) and is the result of volcanic activities which can be dated up to 150000 years ago (Sansivero, n.d.). The bedrock of the eastern part of the island is mainly composed by pyroclastic deposits and lava deposits, while the central-western side is primarily composed by landslide deposits. The bedrock of Mount Epomeo is a green tuff, while its northern slope is made by seabed deposits.
In the last 3000 years, 46 explosive and effusive eruptions have been recorded, of which some were followed by correlated earthquakes (Sansivero, n.d.). Several independent earthquakes have been recorded due to the activity of the PVD, with the last important one recorded in 2017 as 4.0 on the Richter scale (Sansivero, n.d.).

2.4.3. Landslide inventory

As explained in Section 2.4.2, about half of the island sits on a bedrock derived from deposits of landslides and mud flows, indicating that such events have been present since thousands of years. To date, 162 landslides have been recorded in the island, with 18 of these happened since 2003 (Figure 2.3; Bacino Distrettuale, 2025). Most of these landslides are debris flows, earth and rock fall, or slow moving landslides, which indicates that different types of movements are present in the island. Figure 2.4 shows the different types of landslides recorded and their occurrences. Landslides under the field ”Other” did not have a label in the original dataset.

2.4.4. Presence of displacement patterns

To assess whether displacement patterns were present in the island before even conducting any InSAR processing, a research was done on discovering whether any other type of monitoring was carried out. It appears how the Vesuvian Observatory (OV) reports monthly seismic, volcanic and geodetic displacement monitoring to the local Civil Protection (Sansivero, n.d.). 7 GNSS stations are present on the island, roughly evenly scattered in the different domains, with one station close to the summit of Mount Epomeo (Figure 2.6). The timeseries of 2 of these stations are displayed in their monthly reports, and they are displayed in Figure 2.5. As it was not possible to retrieve the raw data for these and the remaining 4 stations, the assessment was made on only these 2 stations.

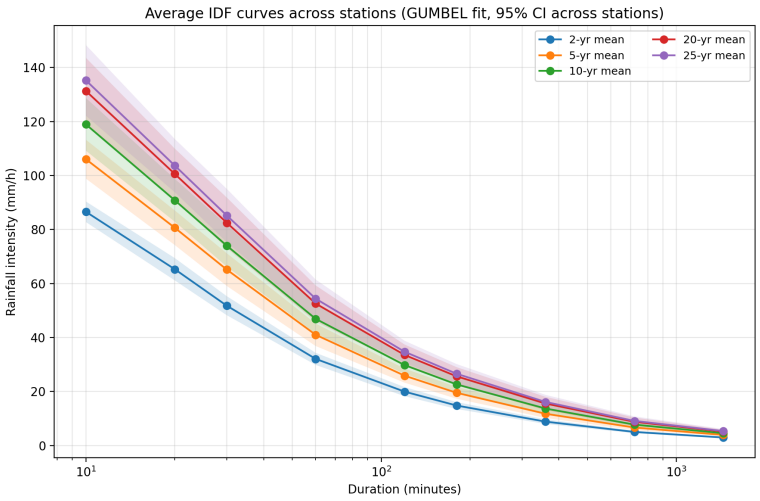

Figure 2.2: Averaged IDF curves across the four stations

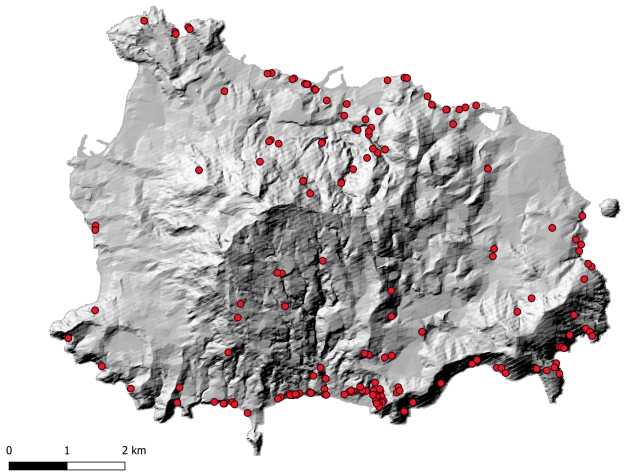

Figure 2.3: Inventory of the recorded landslides (Bacino Distrettuale, 2025)

The timeseries of the Serrara Fontana station (left, centre south of the island) shows a mild displacement of circa $-4mm/yr$ +/- $2mm/yr$, with a seasonal pattern peaking roughly in August, and a seasonal amplitude of $5/10mm$. On the other hand, the Mount Epomeo station (right, mount summit) shows more than double in terms of subsidence ($-10mm/yr$ +/- $3mm/yr$), and a seasonal amplitude of about $15mm$ peaking in winter, possible due to rainfall infiltration and evaporation. The combination of the seasonal patterns and the associated subsidence were used to assess this island as a feasible study area.

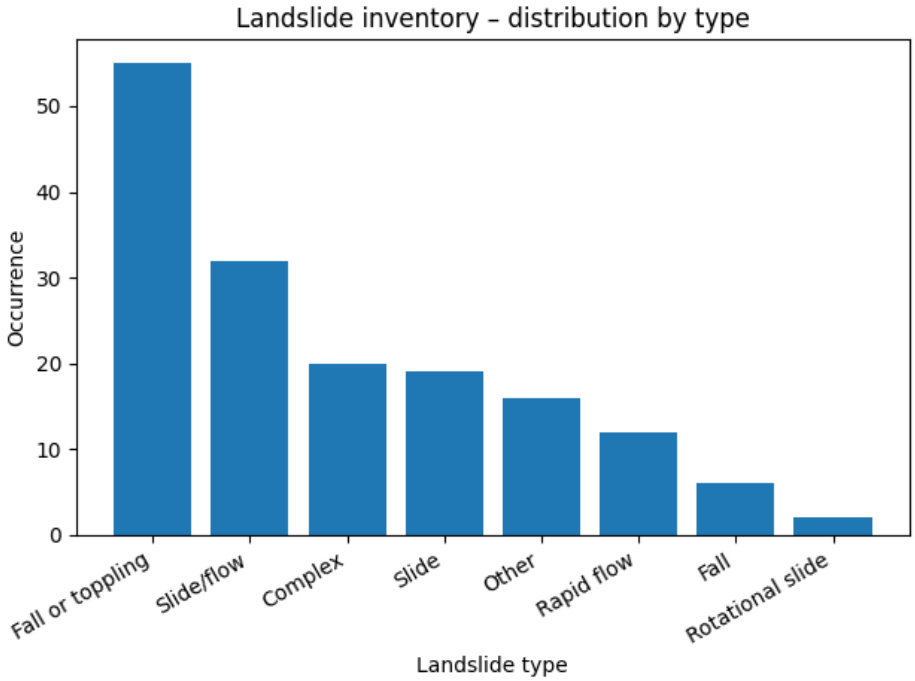

Figure 2.4: Landslide types and occurrences

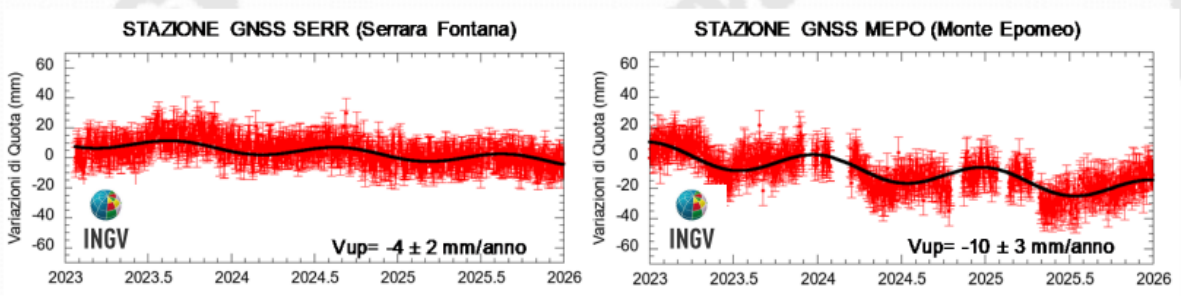

Figure 2.5: 2023 - 2025 timeseries of the 2 GNSS stations at Serrara Fontana and Mount Epomeo (Sansivero, n.d.)

Figure 2.6: Overview of GPS/GNSS locations on the island. Locations with available time series were ”SERR” and ”MEPO” (Sansivero, n.d.)

3

Methodology

This chapter sheds light on the workflow of this project, the data used and the modeling approaches undertaken. Section 3.1 describes the methodology used to create InSAR-derived landslides, including the InSAR processing and analysis methodologies. Section 3.2 describes the static landslides controlling factors used and their retrieval. Section 3.3 describes the LS model architecture for both the model used with only inventory landslides and the model which embraces the InSAR-derived landslides as well. Section 3.4 introduces the study area for this project.

3.1. InSAR-derived landslides

In this research InSAR was used as a tool to derive slopes displacing with a velocity to be considered as ”unstable”, and convert these slopes into an added landslide to the inventory. To achieve this, 6 years of SAR data was processed from 2019 until 2025, to a total of 280 ascending and 279 descending Sentinel-1 images with a 12 days recurrence and a 5*20 m spatial resolution. The data was processed with the processing infrastructure provided by SkyGeo, using the PSI methodology. To derive signal component belonging to the displacement only, corrections for the atmospheric, orbital and topographic component of the signals where undertaken.

3.1.1. InSAR quality parameter selection

Many sources can increase the degree of uncertainty in InSAR and decrease the so-called signal-to-noise ratio (SNR, Hanssen, 2001). Among these we can find temporal decorrelation, which happens when objects on earth give a non consistent backscatter to the radar signal over time (Zebker and Villasenor, 1992). Although the atmospheric signal component is modeled and removed from the displacement signal, extreme atmospheric conditions can still alter the obtained resulting time series, decreasing the SNR (Hanssen, 2001). Other types of errors can be related to the topography estimation, which is inversely proportional to the perpendicular baseline between two acquisitions (Hanssen, 2001). Such errors can lead to a worse estimation of the topographic and phase components, with the resulting issue being topographic phase component being ”leaked” in the displacement phase component.

While the purpose of this work is not to investigate how to remove in all details these uncertainties from the processing side, several post-processing approaches can still be taken to make use only of the InSAR points with a high enough quality. To enhance clarity, from hereon InSAR points can be referred as ”observations”, which should not be confused with the satellite acquisitions over time.

Sensitivity Index

The first step was to filter the observations based on the orientation of the slopes with respect to the line of sight (LOS) of the SAR satellite. Sentinel-1 satellites operate in near polar and sun-synchronous orbit, and emit their signal to the right with respect to the heading direction, at a certain incidence angle with respect to the z-plane. This makes SAR satellites highly sensitive to estimate displacement happening along their LOS vector, therefore they have a higher sensitivity of measuring displacements

on slopes as aligned as possible to the LOS vector. To quantify the sensitivity to monitor the earth's slopes, a so-called Sensitivity Index (SI) was developed, which reflects the projection of the slope-parallel displacement onto the LOS vector (Chang et al., 2018). The SI has values $0 < \mathrm{SI} < 1$, with higher sensitivity when slope and LOS vector are more aligned in the three dimensional cartesian space.

Building upon this work, Van Natijne et al. (2022) developed a freely available SI tool in Google Earth Engine (GEE), which allows to download the SI of Sentinel-1 orbits for the selected areas. This SI is based on the radar's viewing geometry in LOS, and the topography of the terrain over which acquisitions are taken. The topography is included by using the 30m resolution Copernicus Digital Elevation Model (DEM), from which the slope and the aspect are derived. This SI tool already takes into account two more factors related to LOS geometry and topography: shadow, which is the phenomenon typical of a slope in near-vertical direction, where areas at the toe of a slope are obscured by areas at the top, similarly as what happens with optical shadow with respect to the sun; and layover, which corresponds to the phenomenon of two different areas in a slope (crest and toe) being superimposed at the same distance to the radar in the LOS (Van Natijne et al., 2022).

To filter the InSAR observations on only the ones where the estimated velocity can be descriptive of the actual down-slope displacement, the InSAR points were filtered on only the ones overlaying areas with a $\mathrm{SI} > 0.2$ according to the tool developed by Van Natijne et al. (2022). This value was evaluated as a minimum requirement value according to existing literature, where a studies conducted in different areas of the world empirically showed how 0.2 is the minimum value of SI for slope displacement detection using InSAR (Notti et al., 2014; Van Natijne et al., 2022). Furthermore, to have a higher certainty that the remaining points were belonging to non flat areas, only points on a slope of at least $4°$ were kept for the analysis (U.S. Department of Agriculture, Natural Resources Conservation Service, 2022).

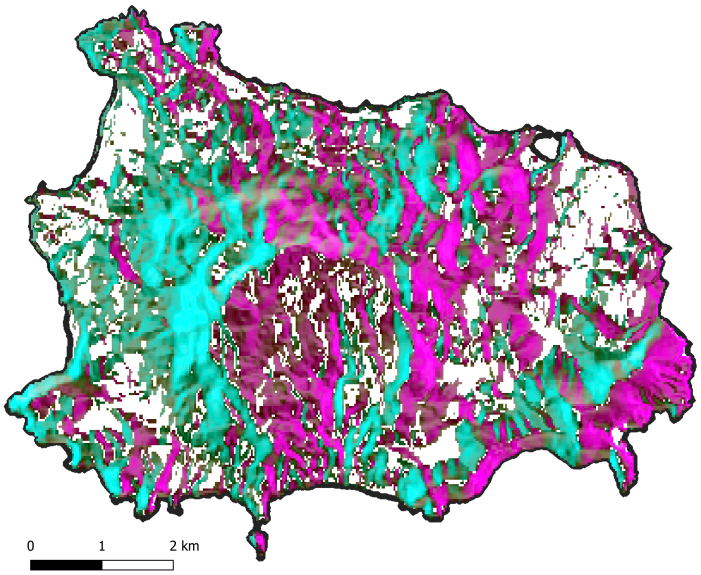

Figure 3.1: Areas with a SI > 0.2. In blue the areas with SI > 0.2 for the DSC track, while in purple the areas with SI > 0.2 for the ASC track

Detectability Power test

InSAR displacements are stochastic, and therefore their estimated displacement should be seen as a PDF (Hanssen, 2001). This leads to the fact that the accuracy of these estimates are related to the standard deviation of the PDFs, and therefore to their SNR. To account for this and only include the InSAR points with a low SNR, a detectability power test was performed. This test is also called the Delft method in existing literature, and is based on the statistical work developed by Teunissen (2024),

and further applied to InSAR analysis by Hanssen (2001) and Kampes (2006). The goal of the test is to eliminate InSAR scatterers whose time series can be explained by just noise in the data, and subsequently to subset the remaining scatterers on the ones that whose true velocity can be estimated with a defined certainty. For clarity, this test will be explained in further depth as divided in two parts: the significance test, and the power test.

Significance test
The significance test has as primary goal to filter the InSAR observations on only the ones whose time series cannot be explained just by pure noise (Kampes, 2006). This is leveraged by conducting a hypothesis test where the null hypothesis H_0 is "no significant displacement is happening", and the alternative hypothesis H_a is "there is significant displacement". Depending on the σ of the displacement (σ_d), a significance level α is chosen as the critical value for which H_0 is rejected. The choice os α is dependent on the amount of Type I errors the user wants to allow for, as a lower α leads to a less strict filter, and some of the remaining time series might still be a result of noise and not actual displacement. For this project, due to time limitations a σ_d was assumed to be $5.5mm/yr$, and α was chosen as $2 * \sigma$. For a deeper explanation on the limitations associated with the σ_d assumption, please consult Section 5.2.2. With the current σ_d and α choices, H_0 would be rejected only for InSAR observations with at least $11mm/yr$ of displacement.

Power test
Based on the significance test, allowing for a high α seems to be the best solution to isolate significant displacement. However, when considering again an InSAR observation as a PDF and recalling to the chosen values for this project, an observation estimated as $12mm/yr$ has almost a 50% chance of being missed, as almost half of the PDF lies on the left side of the $11mm/yr$ significance value. Therefore, a second value β must be considered, which reflects the maximum allowable portion of a PDF to be in the H_0 acceptance zone, which corresponds to a Type II error: a missed detection. Typically, we want to keep this portion as small as possible, given that the consequences of a Type II error are much higher than a Type I error. For this reason, a β value of 5% was chosen, which translates to a velocity of which the PDF's portion in the H_0 acceptance zone is 5%. This velocity is $20.05mm/yr$, which therefore corresponds to the minimum acceptable velocity.

The value of γ, equaling $1 - \beta$, is the detectability power value, and therefore represents the certainty with which it can be said that a certain displacement is estimated. Therefore, the InSAR observations are then filtered further on the ones having a detectability power equal or higher than γ. The InSAR observations which have a detectability power of at least 95% are the ones then used as added landslides to the inventory map, as they show significant displacement and there is a defined certainty for which this displacement is indeed estimated and not missed.

3.2. Landslide susceptibility modeling

To assess the influence of adding the InSAR-derived landslides to the original inventory, a LS model was performed both with only the original recorded landslides and with the inventory augmented with the InSAR-derived landslides. The workflow created is as follows: firstly the static controlling factors were selected, secondly for each grid-cell the controlling factors were stacked, and finally the LS model was trained, tested and used for prediction. Each of these steps are explained in more depth below.

3.2.1. Controlling factors

The static controlling factors chosen for this research were: lithology, soil thickness, terrain wetness index (TWI), slope, aspect, curvature and land use. When possible they were retrieved from local authorities and research centers, such as lithology and land use (Bacino Distrettuale, 2025), rainfall ("Centro Funzionale Multirischi di Protezione Civile Regione Campania", n.d.) while the others were calculated from a 10m-resolution DEM (Tarquini et al., 2022). For the factors that had a different spatial resolution, a nearest-neighbor up-sampling was conducted to not lose the information contained in the finer raster layers.

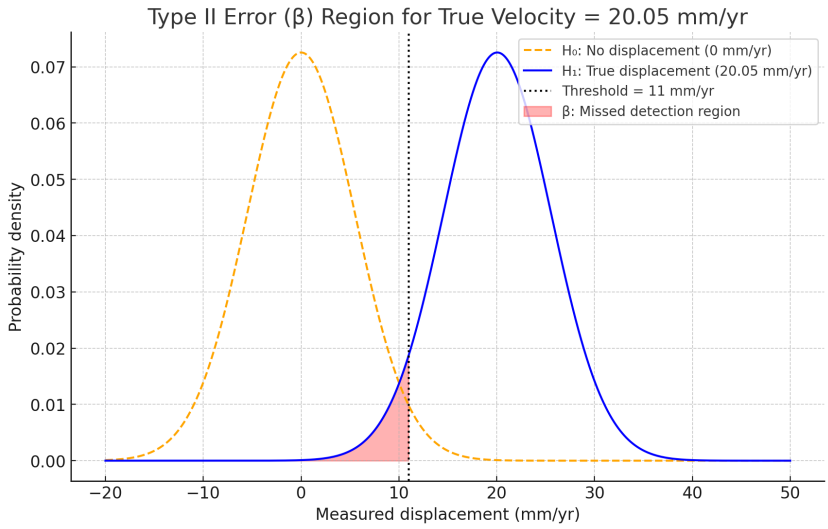

Figure 3.2: PDF with a detectability power of at least 95%

Soil thickness was one of the controlling factors that was not readily available, and had to be derived. A research by De Vita and Nappi (2013) derived an empirical relationship between soil thickness and slope angle, for angles > $28°$. The research was conducted on the island of Vivara, located 5 km away east of Ischia. From a measured soil thickness $5 < m < 20$ across areas where the slope is $0°$, the following formula was applied to derive the thickness z in steeper areas:

$$z = z_0 \cos(\alpha), \quad \alpha > 28° \tag{3.1}$$

where z_0 is the thickness at on flat areas, and α is the slope angle. In the absence of local data, it was assumed a value of 5m soil thickness in flat areas, and Eq. 3.1 was used to calculate the soil thickness of Ischia. This assumption was made on the basis that the islands have similar geologic origins, although this may lead to over/underestimating soil thickness in areas of the island where this slope - thickness relationship may not hold.

Rainfall data was collected in 10-minutes intervals and resampled to compute yearly averages from the 4 recording stations. The yearly averages were computed from the years of deformation investigated. Thiessen polygons were used as spatial interpolation method, where the rainfall value of the closest station was assigned.

A correlation test between the controlling factors was performed, to make sure that each controlling factor could provide distinct information to the landslide susceptibility model. The decision of the correlation coefficient choice was based on 2 factors: the distribution type of each controlling factor, and the expected correlation type of the controlling factors. The PDF of each controlling factor showed how none of them is normally distributed, with only slope, TWI and Terrain Roughness Index (TRI) being positively skewed, while the other controlling factors could not be classified. Furthermore, some controlling factors are independent from each other, such as landuse and lithology, while others were calculated from the slope or DEM with non-linear equations. This can indicate the presence of correlations between the controlling factors, which together with the non-gaussian distributions lead to the choice of using the Spearman correlation coefficient (De Winter et al., 2016). The correlation table present in Appendix 1 shows how the TRI had high correlation coefficients with slope and soil thickness, therefore this was further investigated by using a Variance Inflation Factor (VIF) test. The VIF computes for each factor the multicollinearity with other factors by regressing it against all other factors in such a way:

$$VIF_j = \frac{1}{1 - R_j^2} \tag{3.2}$$

Where R_j^2 is the regression factor between one controlling factor and all the other ones. Controlling factors with a VIF value > 5 would be omitted from susceptibility modeling. The initial test brought

a value of ~22 for slope and ~30 for TRI, and by omitting TRI it was seen how the slope's VIF value would drop to 5.1 (Table 3.2; Table 3.1). This led to the decision of omitting TRI from the susceptibility modeling and keeping the slope, as a value closely around the threshold was considered acceptable.

Table 3.1: VIF values (with TRI)

Factor	VIF
Slope	22.21
TWI	1.71
TRI	29.82
Curvature	1.07
Aspect	1.02
Soil thickness	5.76
Landuse	1.13
Lithology	1.03
Rain	1.03

Table 3.2: VIF values (without TRI)

Factor	VIF
Slope	5.07
TWI	1.71
Curvature	1.07
Aspect	1.02
Soil thickness	3.83
Landuse	1.13
Lithology	1.03
Rain	1.02

Therefore, the Spearman correlation test was conducted among the above-mentioned controlling factors excluding the slope, as shown in Figure 3.3. The correlation matrix shows no correlation across all variables, except some moderate to strong correlation between slope, soil thickness and TWI. However, the VIF test conducted showed values <= 5, which led to the choice of keeping all these controlling factors (Table 3.1).

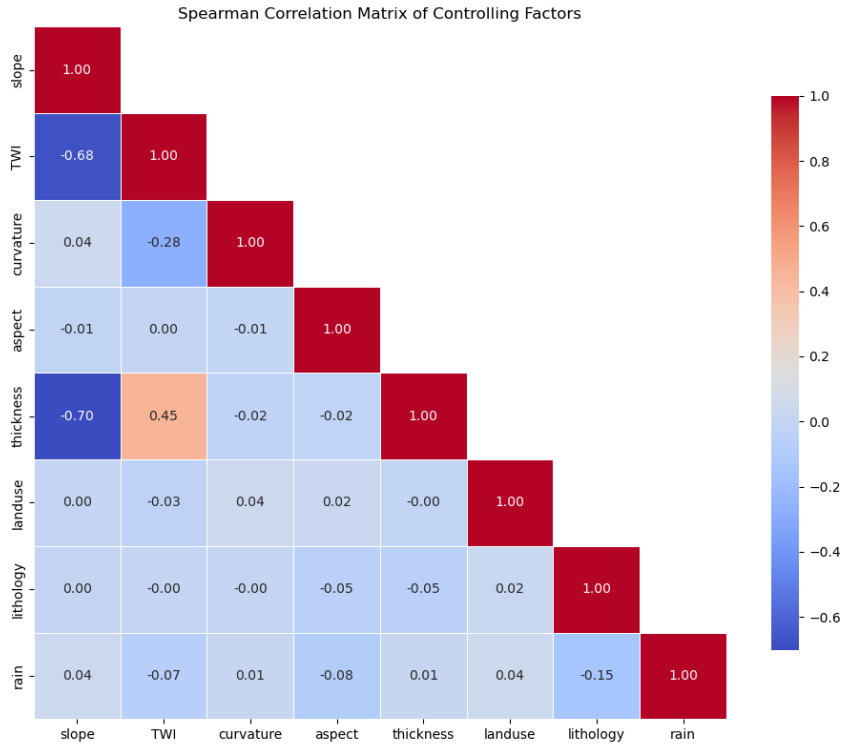

Figure 3.3: Spearman correlation matrix

3.2.2. LS model set-up

All spatial datasets (vector and raster) representing the controlling factors and landslide inventory were projected to a common coordinate reference system. Each factor was then resampled to match the 10 m resolution of the DEM, which represents the finest spatial resolution among all variables. Datasets with coarser resolution were upsampled using nearest-neighbor resampling. As a result, each grid cell

within the area of interest (AOI) contains a value for every controlling factor, as well as a binary indicator denoting whether a landslide occurred (1) or did not occur (0).

Following dataset preparation, the modeling phase was conducted. The dataset was divided into training and testing subsets using an 80%–20% split. Cross-validation was applied to iteratively train and evaluate the model across multiple train–test partitions, ensuring that the full dataset was utilized without being processed all at once. This approach allows the model to be trained on different subsets of the data repeatedly and reduces the risk of overfitting (Berrar, 2019).

However, the dataset is highly imbalanced, with more than 400000 grid cells but only 162 representing landslide occurrences. Under such conditions, a model would tend to predict the majority class ”0”-no landslide for all cases. To address this issue, the dataset was balanced by sampling the ”0” and ”1” classes in a 1:2 ratio during both training and testing. This enables the model to better learn the relationships associated with landslide occurrence. Class balancing is a common practice in landslide susceptibility modeling, given the typical imbalance in spatial datasets (Lombardo and Mai, 2018; Reichenbach et al., 2018). Commonly used ratios include 1:1, 1:2, and 1:3; in this study, a 1:2 ratio was selected as a compromise between model performance and computational efficiency, since a 1:1 ratio resulted in excessive processing time.

In the machine learning framework, the controlling factors serve as input variables, while the binary landslide indicator (0/1) represents the target variable. During training, the model learns the relationships between the controlling factors and landslide occurrence. These learned relationships are subsequently used to predict, for each grid cell in the testing dataset, the probability (ranging from 0 to 1) of landslide occurrence.

This continuous probability is then converted into a binary classification (0 or 1) using a predefined threshold, which in this study was set to 0.5. This value is commonly adopted in LS modeling, particularly in both statistical approaches and machine learning frameworks, as it represents the default decision boundary in many binary classification algorithms (Catani et al., 2013; Zhou et al., 2021). However, it should be noted that the selection of a fixed threshold is inherently arbitrary and may not be optimal for all study areas, as it depends on the specific data distribution and the relative importance of false positives and false negatives. Alternative approaches, such as threshold optimization based on ROC or precision–recall analysis, have been proposed in the literature, but a universally accepted standard for threshold selection in LS modeling has not yet been established.

Once having trained and tested the model having computed the relevant testing metrics, the model with the highest metrics was chosen to predict LS over the entire AOI. This is still predicted as a $0 \sim 1$ probability, which was then sub-divided in three classes: **low** ($p < 0.33$), **medium** ($0.33 < p < 0.66$) and **high** ($p > 0.66$). In the existing literature, three, four, or five susceptibility classes are generally proposed, and the decision of three classes was made to easily compare the resulting susceptibility map to the one used by the local authorities, which also uses three susceptibility classes (Bacino Distrettuale, 2025; Reichenbach et al., 2018).

This modeling procedure was executed two times: the first model was performed with only the recorded landslides and no rainfall among the controlling factors, which from hereon will be addressed as the ”Traditional” model; the second model with the InSAR-augmented inventory (recorded + InSAR-derived landslides) and the addition of rainfall among the controlling factors. This was done for two specific reasons: to create a benchmark comparison for the InSAR-augmented LS model, and to test whether a hydrological factor such as rainfall could be suitable to explain slope instability over the island.

3.3. Model performance assessment

The model performance will be evaluated with a Receiver Operating Characteristic (ROC) curve, frequently used in LSM (Guzzetti et al., 2012; Reichenbach et al., 2018). By calculating the Area Under the Curve (AUC) of the ROC curve, the overall performance is evaluated, with values closer to 1 representing better performance. In general terms, the AUC can be interpreted as the probability that a

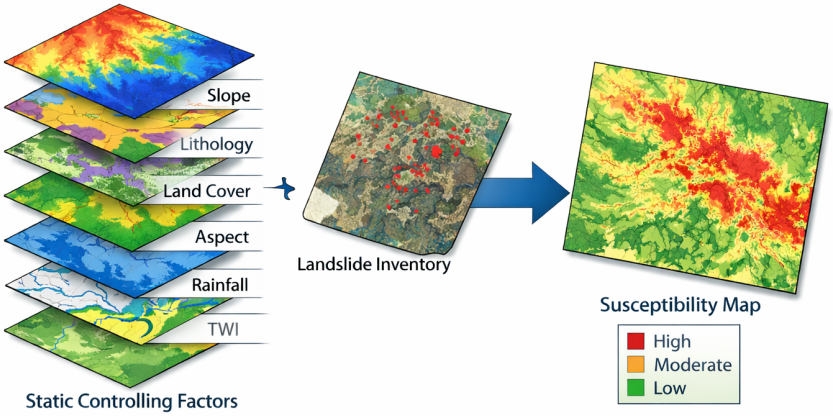

Figure 3.4: Graphical visualization of the LSM

classifier gives a randomly chosen landslide sample an unstable classification. Therefore, a higher value represents a higher probability of correct classification. Other metrics used for model performance assessment are:

$$Recall = \frac{TP}{TP + FN} \tag{3.3}$$

$$Precision = \frac{TP}{TP + FP} \tag{3.4}$$

$$F1 - Score = \frac{2 * Precision * Recall}{Precision + Recall} \tag{3.5}$$

Relative importance will be given to the recall metric, as it is important in the case of highly costly Type II errors (false positives), which is the case for landslides as lives and critical infrastructure can be affected. On the other hand, precision comes to importance when the concern for Type I errors (false positives) is higher than Type II errors, which does not represent the environmental problem in question. However, it can still provide insights on model performance, and it is needed to compute the F1-Score, a harmonized metric where models with different precision and recall values.

4

Results

This chapter shows the results related to the creation of the InSAR derived landslides (4.1), and the LS modeling results, where both metrics are shown and resulting LS maps are displayed.

4.1. InSAR-derived landslides

As explained in Section 3.1.1, the processed InSAR points was first filtered based on their location, whether they were in a location with a $SI > 0.2$ *and* on a slope of at least $7°$; then based on their displacement velocity, with only the scatterers showing at least a $20.05mm/yr$ velocity being included in the InSAR-derived landslides.

From Table 4.1 it can be seen how roughly 0.3% of the scatterers have a velocity higher than the $11mm/yr$ threshold, and only around 1/3 of those have a displacement velocity higher than $20.05mm/yr$. This leaves a total of 321 InSAR scatterers, which overlayed on the 0.2 SI and the at least $4°$ slope leads to 129 InSAR-derived landslides.

Table 4.1: Percentage of remaining InSAR scatterers used to generate the InSAR-derived landslides

	ASC	**DSC**
Original scatterers	99449	77023
Reject H0	515 (0.5%)	439 (0.56%)
Scatterers [detect. Power] > 95%	157 (0.16%)	164 (0.21%)
Scatterers overlaying SI > 0.2	75 (0.07%)	79 (0.1%)
Scatterers over a slope > $4°$	62 (0.06%)	55 (0.08%)

It should be noted that the $20.05mm/yr$ velocities are still in LOS, the satellite's viewing geometry. As not all slopes are parallel to the LOS, this is only a portion of the down-slope displacement velocity. To have an overview of the actual magnitudes of down-slope displacement velocities, the LOS velocities were re-projected to align with the down-slope vector. This was done by using two environmental parameters, slope angle and aspect, and two satellite parameters, the incidence angle and heading angle.

A three-dimensional trigonometrical re-projection was applied, and the resulting velocities are as expected higher than the LOS velocities. Figure 4.1 shows how the majority of the estimated down-slope velocities lie below $125mm/yr$, with extreme values stretching up to $190mm/yr$. The landslides derived from the descending InSAR track appear to be less scattered than the ones derived from the ascending track.
Figure 4.2 shows the distribution of the inventory and InSAR-derived landslides. It can be seen how the north and eastern areas are populated by InSAR landslides from the ASC track, which is intuitive as slopes in that area look in the LOS direction. Due to local slopes, there is no clear pattern of distribution for the landslides derived from the DSC track. The count of total landslides is now 162 inventory landslides + 117 InSAR-derived landslides = 279 total landslides.

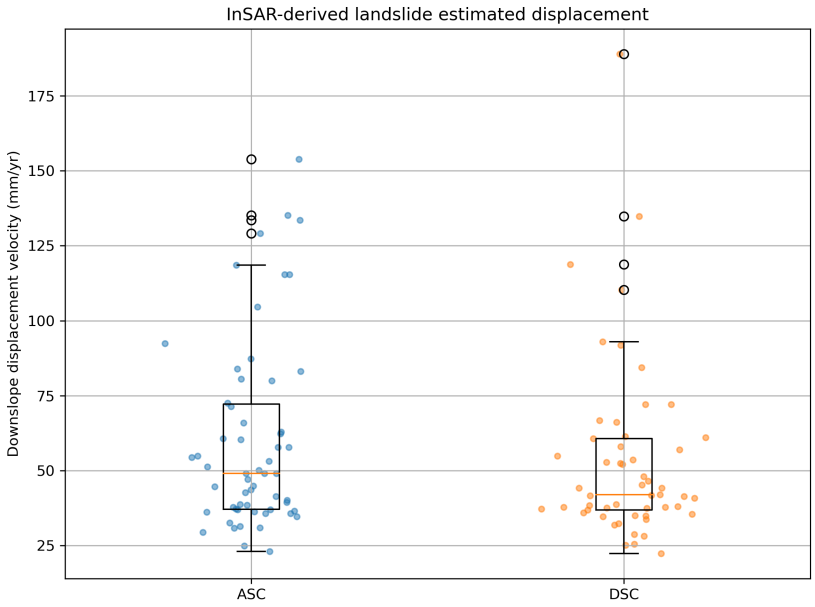

Figure 4.1: Distribution of velocities of the InSAR scatterers used for the InSAR-derived landslides

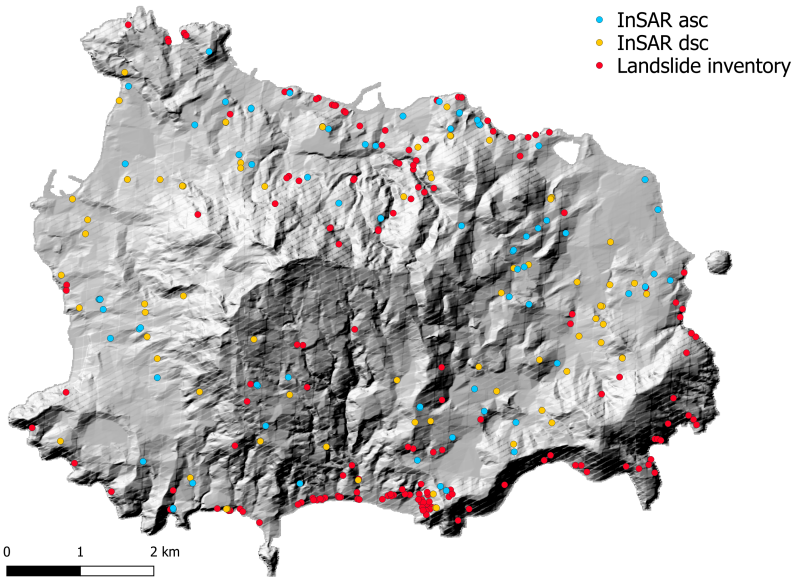

Figure 4.2: Overview of all the landslides, including inventory and InSAR-derived

4.2. Landslide Susceptibility modeling

4.2.1. Susceptibility modeling metrics

An in-depth evaluation of the traditional LS model and the InSAR-augmented model was conducted for both XGB and RF algorithms. Overall, the traditional models exhibit moderate performance, with F1-scores not exceeding 0.63, AUC values up to 0.81, and Recall values reaching a maximum of 0.56.

Considering the best-performing models from cross-validation and using the F1-score as the primary evaluation metric, the InSAR-augmented XGB model slightly outperforms the best traditional model, achieving an improvement of 0.06. A similar trend is observed in the AUC scores, although the increase of 0.02 is relatively minor in relation to the overall metric values (Tables 4.2; 4.3). Notably, the InSAR-augmented model yields a Recall approximately 10% higher than the traditional model. However, with a Recall of 0.57, it still fails to identify 43% of landslide events, indicating a substantial proportion of false negatives.

From the ROC curve comparison in Figure 4.4 it can be seen how the InSAR-augmented LS model has a higher performance at all false positive rates, especially between $0.2 < FPR < 0.4$. This is a signal of a more robust model in terms of false alarming, which in this case translates to a low probability of predicting ”0” areas as landslides (”1”).

When inspecting the traditional LS model results over the testing iterations, it appears how the XGB model shows higher variance in every score with respect to the RF model, while this is not the case for the InSAR-augmented LS model. In fact, the RF in the InSAR-augmented model shows higher variance in Precision, Recall and F1-Score, but not in AUC score. When inspecting median scores, it appears how the two LS models are almost equivalent, with differences up to 5% in median scores (Figures 4.3a, 4.3b).

Table 4.2: Metrics of the best traditional LS model based on F1-Score

Metric	XGB	RF
AUC	0.75	0.73
Precision	0.68	0.66
Recall	0.48	0.48
F1-Score	0.57	0.56

Table 4.3: Metrics of the best InSAR-augmented LS model based on F1-Score

Metric	XGB	RF
AUC	0.77	0.81
Precision	0.69	0.71
Recall	0.57	0.46
F1-Score	0.63	0.56

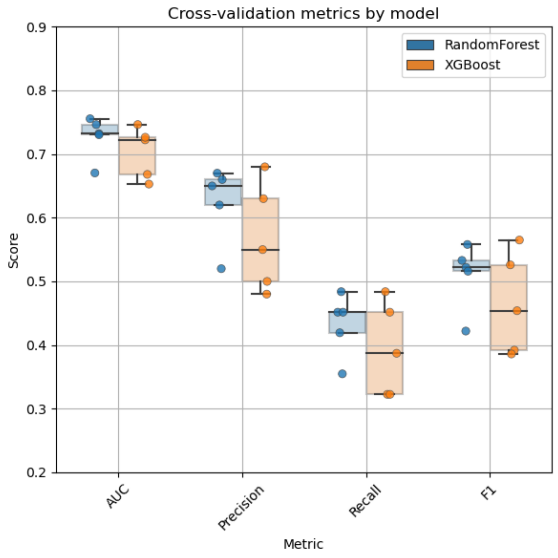

(a) Scores distribution of the traditional LS model

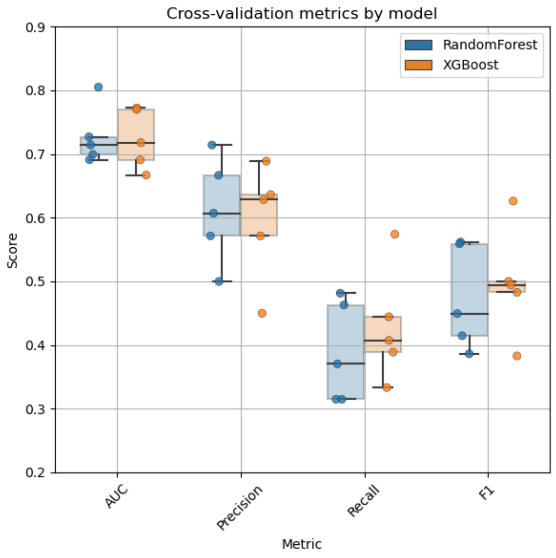

(b) Scores distribution of the InSAR-augmented LS model

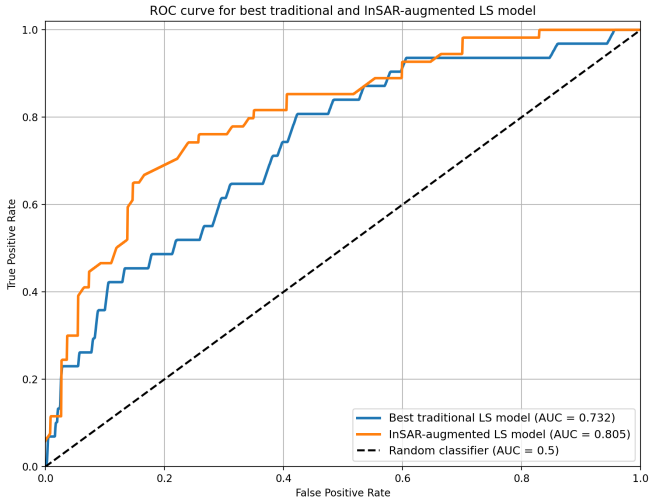

Figure 4.4: ROC curve for best traditional and InSAR-augmented LS model

Furthermore, Figure 4.5a highlights the number of TP, TN, FP and FN. It can be seen how the roughly 10% of the landslides samples have been missed in the traditional LS model, as 17 FN are present out of 162 landslide samples. With this assessment the TN percentage is around 9%. With the InSAR-augmented model, the FN percentage remains in line with the previous model: 10% of the landslide samples appear as missed landslides (28 out of 279; Figure 4.5b).

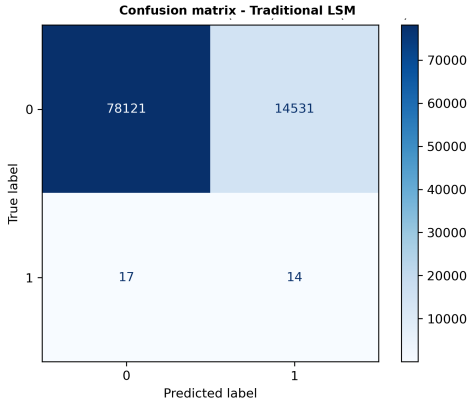

(a) Prediction confusion matrix of the traditional LS model

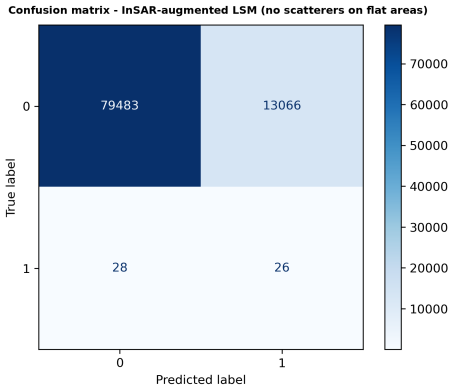

(b) Prediction confusion matrix of the InSAR-augmented LS model

4.2.2. Resulting Landslide Susceptibility Map

LS maps were generated from the traditional and InSAR-augmented models with the highest F1-Score. Table 4.4 shows that the two maps differ across all susceptibility classes, with deviations of 6% in the Low class, 18% in the Medium class, and 20% in the High class. These differences are consistent with the visual patterns observed in Figure 4.6. In particular, the InSAR-augmented LSM predicts a larger extent of Medium susceptibility, whereas the traditional LSM assigns greater areas to both Low and High susceptibility classes.

Table 4.4: Comparison of susceptibility classes between Traditional LSM and InSAR-augmented LSM

Susceptibility class	Traditional LSM	InSAR-augmented LSM
Low	320609	301269
Medium	114539	139226
High	28263	22519

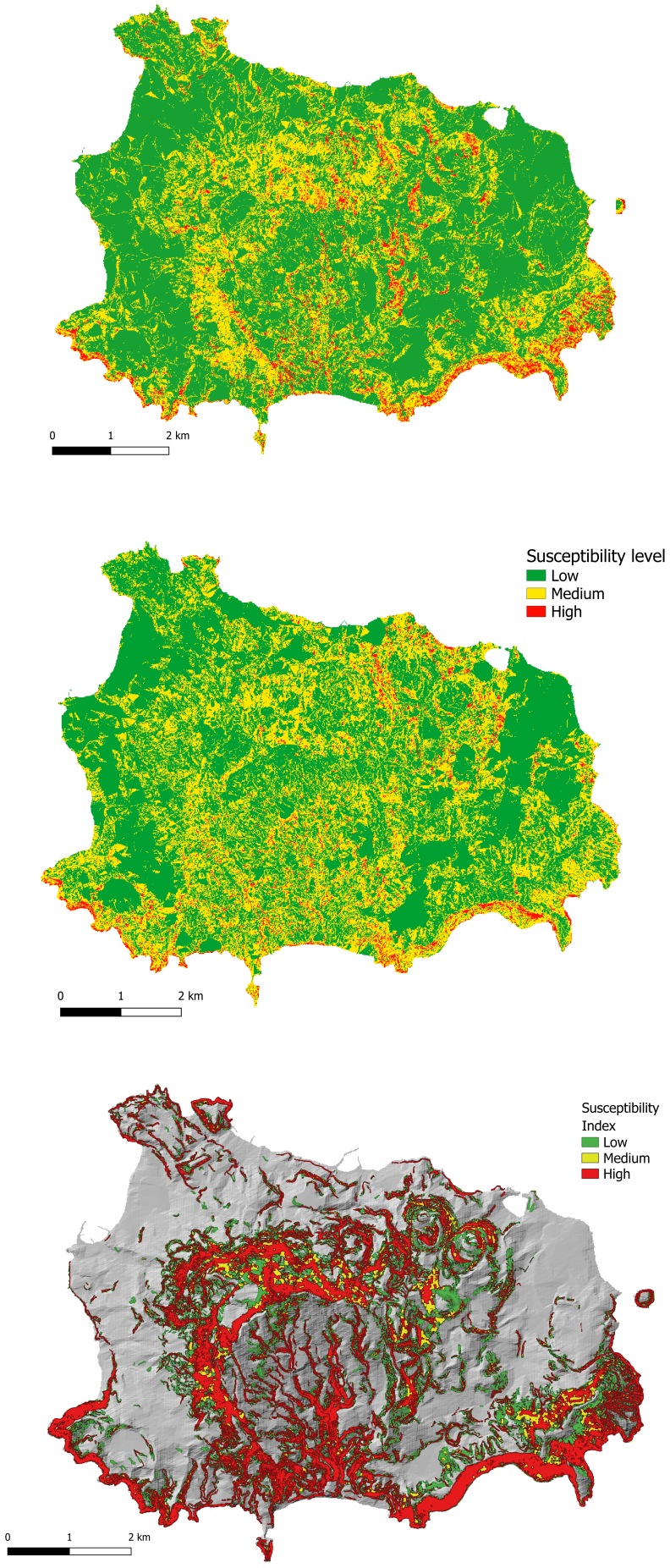

Figure 4.6: Comparison of the LS map achieved with the traditional LS model (top), InSAR-augmented LS model (center), and map used by the local authority (bottom; Bacino Distrettuale, 2025)

5

Discussion

Given the amount of points of discussion present, they will be divided in two main sections: the first one including the discussion points regarding the methodology used, while the second one which includes the discussion on the results obtained.

5.1. Selection of study area

The first discussion point starts with the selection of the study area, where several features can play an important role in the study area decision. For this study, initially other areas were identified, such as the area surrounding the Partenio Regional Park in Campania, Italy, roughly 30km east of the city of Naples. Here the challenges encountered through the InSAR processing due to the high vegetation and the resulting displacement patterns observed made the park a non suitable location for such a study, and such challenges can be extrapolated to general challenges when wanting to use InSAR-augmented LSM.

Notwithstanding it being an area with several landslides happened in the past, the park and its surrounding slopes showed no movement except for a +/- $10mm$ seasonal displacement. Furthermore, the size of the landslides present in the area, such as the one happened in San Martino Valle Caudina in 2019 with an area of roughly 3 hectares of failed soil, creates more challenges for InSAR to even capture such substantial changes in the surface.

5.2. Methodology Discussion

5.2.1. InSAR processing methodology

For this study initially the InSAR data was processed both by using the PSI and SBAS methodologies. These two delivered similar results in terms of magnitude of displacement, however there were different results in the trends that were captured. The resulting PSI time series appeared to be smoother in time, while the SBAS time series showed more prominent irregular patterns. Although this initially made the SBAS output more suitable for this research, as these irregularities could be attributed to possible hydrological factors, the lower coverage in the SBAS output directed the choice to the PSI output.

However, it shall be noted that the non-linear trends found in the SBAS timeseries and the local GNSS stations led to the indication of possible soil-water interaction, and therefore led to the choice of rainfall as a non-static controlling factor.

5.2.2. InSAR analysis assumptions

The Detectability Power test performed in Section 3.1.1 lies on the assumption of having a constant standard deviation of the velocity of $5.5mm/yr$. However, this decision was made due to time limitations and because it was attributed that the derivation of this value was outside the scope of this research, and in reality each scatterer presents its own standard deviation. This is is not computed by fitting a model

through the resulting timeseries, but it shall be computed by starting from the phase variance. This is a first estimation of the correlation through time of a scatterer, and its coherence is inversely correlated to the phase variance. The use of this parameter can provide further insights on the quality of the produced timeseries, however a workflow on its spatial distribution shall be made. While the resulting velocity standard deviation can be taken from each scatterer, the choice of the *alpha* and *beta* values should be taken on sub-AOIs. This is because each sub-region might have different tolerances of missed detections, for instance regions with socially critical infrastructure downslope such as hospitals.

5.2.3. Use of displacement thresholds

By using the methodology as explained in Section 3.1.1, all the InSAR scatterers with displacement rate greater than $20.05mm/yr$ were considered as "unstable" scatterers, therefore they were added to the landslide dataset. However, a distinction must be made between all the scatterers that have a >95% detectability power threshold, and areas that are actually unstable.

The detectability power test filters InSAR data on scatterers whose timeseries cannot only be explained by the noise, and therefore there is indeed displacement happening, and there is a specified minimum certainty that this displacement is indeed captured. On the other hand, the goal of this research was to leverage InSAR technology to assess whether scatterers would lay on unstable slope, and use those to expand on the local landslide inventory dataset. In this regard, the detectability power threshold derived in Section 3.1.1 may technically not represent the threshold of the difference between a stable and an unstable area. Chen et al. (2023) Feng et al. (2025) proposed a methodology which is based on the delineation of displacement thresholds, which could possibly be used as an addition of the detectability power test. Thus, a possible future use of this methodology could see the expansion of the detectability power test including the use of the phase variance to derive the displacement standard deviation, and thereafter still using displacement thresholds to actually select the displacement that supposedly belongs to unstable slopes.

5.3. Results Discussion

5.3.1. Controlling factor importance

Inspection of the susceptibility maps produced by the two modelling approaches already suggests a shift in the relative importance of the controlling factors. To investigate this more systematically, a SHAP analysis was conducted over the entire AOI for each modelling scenario. Because SHAP provides a heuristic ranking of feature importance without an associated significance test, an additional bootstrap-based comparison was performed. Specifically, 300 sub-samples of the AOI were generated and, for each sample, the relative SHAP importance of selected factors was compared. This allowed to evaluate how consistently one factor ranked above another across the study area.

Traditional LS model

For the traditional LS model, the SHAP analysis indicates that slope is the most important controlling factor, followed by soil thickness and TWI (Figure 5.1). The dominant role of slope is consistent with previous landslide susceptibility studies, which commonly identify topographic and hydrological variables—including slope, elevation, and wetness-related indices—as among the most influential predictors (Chang et al., 2018; Guzzetti, 2000; Reichenbach et al., 2018).

The bootstrap analysis supports this interpretation. Across all 300 sampled sub-portions of the AOI, slope showed higher global SHAP importance than thickness (Table 5.1). This suggests that the dominance of slope over thickness is spatially robust within the study area.

Table 5.1: Bootstrap-based comparison of SHAP global importance between selected conditioning factors for the traditional LS model.

Feature comparison	$\mathbf{P(Sl > Th)}$	Mean difference	95% CI
Slope > Thickness	1.000	0.0437	[0.0432, 0.0444]

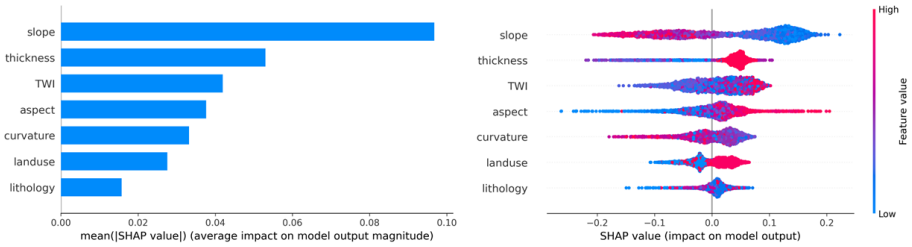

Figure 5.1: SHAP values for the controlling factors of the traditional LSM.

InSAR-augmented LS model

For the InSAR-augmented LS model in which scatterers on flat areas were excluded, the SHAP analysis shows slope and land cover as the two most important controlling factors (Figure 5.2). Although both variables appear highly influential, the bootstrap comparison indicates that slope consistently ranks above land cover across all 300 AOI samples (Table 5.2). Therefore, slope can still be considered the most dominant controlling factor in this model configuration. This result suggests that, after filtering InSAR-derived landslides to slope areas, the model retains a geomorphologically plausible structure, with slope remaining the primary predictor while land cover becomes more relevant than in the traditional LS model.

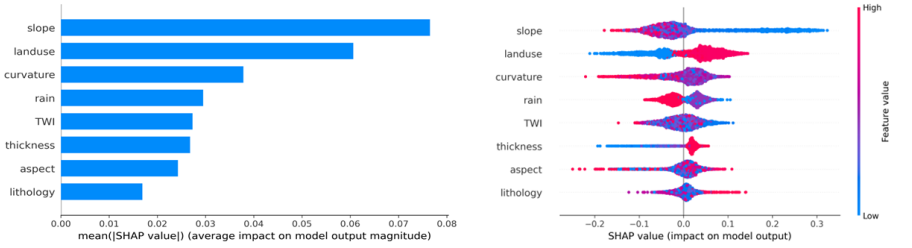

Figure 5.2: SHAP values for the controlling factors of the InSAR-augmented LSM without scatterers on flat areas.

5.3.2. Importance of filtering InSAR points on slopes

To assess the influence of including scatterers located on relatively flat areas, an additional InSAR-augmented LS model was trained using the full InSAR-derived inventory, while keeping all other modelling settings unchanged. The resulting performance deteriorated compared with the slope-filtered InSAR model, particularly for Recall and F1-score, whereas other metrics changed only marginally (Table 5.3). This indicates that including flat-area scatterers introduces noise or reduces the geomor-

Table 5.2: Bootstrap-based comparison of SHAP global importance between selected conditioning factors for the InSAR-augmented LS model without flat-area scatterers.

Feature comparison	$\mathbf{P(Sl > LC)}$	Mean difference	95% CI
Slope > Land cover	1.000	0.016	[0.015, 0.017]

phological consistency of the inventory, thereby weakening model performance.

Table 5.3: Performance metrics of the InSAR-augmented LS model with all InSAR-derived landslides.

Metric	XGB	RF
AUC	0.70	0.70
Precision	0.66	0.70
Recall	0.38	0.34
F1-Score	0.48	0.46

The SHAP analysis of this unfiltered InSAR-augmented model shows a substantial change in the ranking of controlling factors. In contrast to the traditional LS model, where land cover ranked among the least important variables, land cover becomes the most important factor here, followed by curvature (Figure 5.5). This pattern is not fully consistent with the literature, which more commonly identifies slope, hydrology, and elevation-related variables as dominant predictors (Kassa et al., 2024; Pradhan et al., 2023; Meena et al., 2022; Reichenbach et al., 2014). Two factors may explain this result.

1. **InSAR scatterers are preferentially located on artificial structures.** Because C-band SAR coherence is typically poor over vegetated terrain (Zebker and Villasenor, 1992), persistent scatterers are more likely to be associated with buildings, roads, and other man-made structures, with only a limited number of scatterers occurring over exposed rock in the central part of the island. If a substantial proportion of the InSAR-derived landslide inventory is therefore associated with urbanised areas, it is reasonable that land cover emerges as a highly influential predictor.

2. **Land cover resolution and positional uncertainty may affect class attribution.** The positional uncertainty of the satellite observations (approximately ± 5 m) combined with a land cover raster resolution of 10 m increases the likelihood that some scatterers are assigned to an incorrect land cover class. Visual comparison between the land cover raster and optical imagery shows that small-scale heterogeneities are not always captured. For example, small terraces, gardens, and vegetated patches adjacent to houses and roads may still be classified as urban fabric (Figure 5.3).

The bootstrap analysis confirms the strong influence of land cover in this model configuration. Across all 300 sampled AOI sub-portions, land cover consistently ranked above curvature (Table 5.4). This indicates that the dominance of land cover is not a local artefact, but a spatially persistent feature of the unfiltered InSAR-based inventory.
Overall, these results highlight the importance of filtering InSAR-derived points according to slope conditions before using them to construct landslide inventories. Without this filtering step, the model appears to incorporate signal related to sensor sampling characteristics and land cover representation rather than landslide-controlling geomorphological processes alone.

Table 5.4: Bootstrap-based comparison of SHAP global importance between selected conditioning factors for the InSAR-augmented LS model with scatterers on flat areas.

Feature comparison	$\mathbf{P(LC > Cu)}$	Mean difference	95% CI
Land cover > Curvature	1.000	0.010	[0.009, 0.010]

Figure 5.3: Example of possible InSAR scatterers overlapping pixels classified as urbanised land cover (red), although they may actually belong to other local land cover classes.

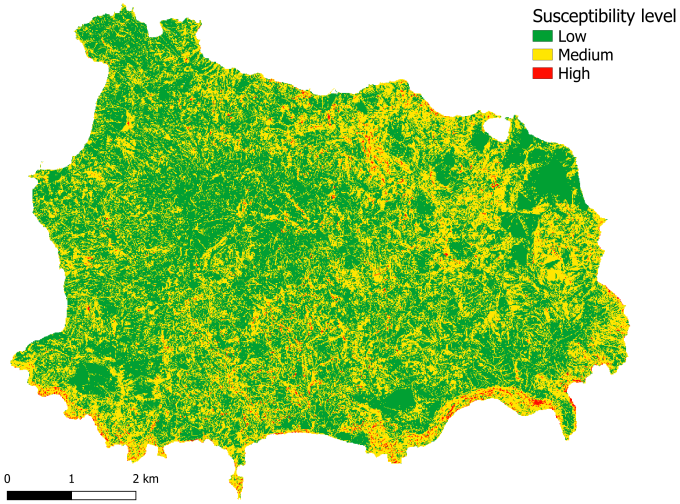

Figure 5.4: Susceptibility map resulting from the InSAR-augmented LSM with scatterers on flat areas.

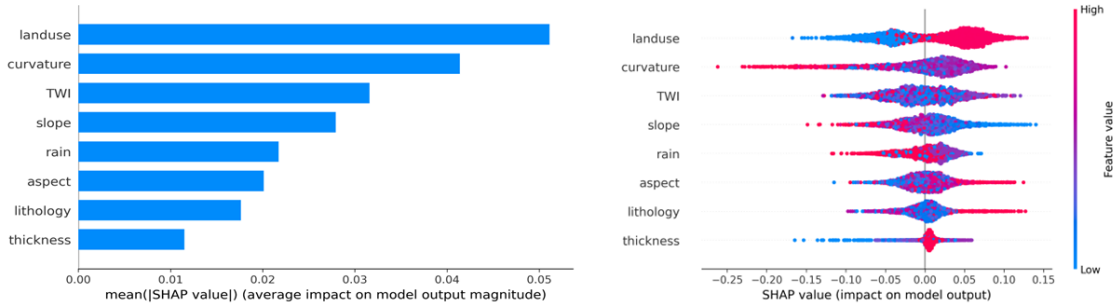

Figure 5.5: SHAP values for the controlling factors of the InSAR-augmented LSM with scatterers on flat areas.

6

Conclusion

This research evaluated the integration of InSAR-derived surface deformation into landslide susceptibility modelling by comparing three modelling approaches: a traditional susceptibility model based on established controlling factors, an InSAR-augmented model using slope-filtered deformation points, and an augmented model including all InSAR-derived points without additional geomorphological filtering.

The comparison between the traditional model and the slope-filtered InSAR-augmented model demonstrates that InSAR-derived information can be incorporated into landslide susceptibility modelling without compromising its physical basis, provided that deformation signals are constrained to slope areas. In both models, slope remains the dominant controlling factor, followed by soil thickness and hydrological proxies, indicating that the susceptibility patterns are still governed by terrain conditions consistent with rainfall-induced landslide processes in the study area.

At the same time, the inclusion of slope-filtered InSAR-derived landslides leads to a measurable shift in the relative importance of certain predictors, particularly land cover. This suggests that InSAR data introduce additional spatial information related to surface characteristics and observation conditions. However, as long as slope remains the primary controlling factor, this shift does not compromise the geomorphological interpretability of the model, but rather reflects the combined influence of terrain and observation-driven sampling.

A contrasting behaviour is observed when InSAR-derived points are included without applying slope-based filtering. In this case, model performance decreases, particularly in recall and overall predictive capability, and the ranking of controlling factors changes substantially. Land cover becomes the dominant predictor, while slope loses its primary role. This indicates that the model is no longer capturing landslide-related processes, but is instead learning patterns associated with the spatial distribution of InSAR scatterers, especially in urbanized and low-slope areas.

These results highlight a critical distinction: even when InSAR data are processed using standard quality criteria and include an initial slope constraint, this is not sufficient to ensure that the detected deformation corresponds to slope instability. The additional test without slope filtering clearly shows that the inclusion of deformation signals from flat or weakly sloping terrain introduces non-landslide-related processes, which degrade both model performance and physical interpretability.

The key finding of this study is therefore that the value of InSAR-derived deformation in landslide susceptibility modelling lies not in its direct incorporation, but in its selective integration under strict geomorphological constraints. When InSAR-derived points are restricted to slope areas, they can complement traditional landslide inventories while preserving the fundamental role of slope as the main controlling factor. When this constraint is not applied, the integration fails to improve the model and can even lead to misleading susceptibility patterns.

Overall, this research demonstrates that InSAR data should not be treated as a straightforward extension of landslide inventories, but as a conditional data source whose usefulness depends on how deformation signals are filtered and interpreted. The comparison between filtered and unfiltered approaches provides clear evidence that geomorphological consistency—particularly the enforcement of slope conditions—is a necessary requirement for the successful integration of InSAR into landslide susceptibility modeling.

6.1. Recommendations

Based on the findings of this study, several recommendations can be made to improve the integration of InSAR-derived deformation into landslide susceptibility modelling.

The results clearly show that including InSAR-derived points from low-slope areas leads to a degradation of model performance and a loss of physical interpretability. Therefore, slope-based filtering should not be considered an optional refinement, but a necessary preprocessing step when using InSAR data for inventory augmentation. Only deformation signals occurring on sufficiently steep terrain should be considered as potential indicators of slope instability.

Although a minimum slope threshold was applied in this study, the results suggest that a single, fixed threshold may not be optimal for all environments. Future research should investigate adaptive or region-specific slope thresholds that account for local geomorphology, landslide types, and triggering mechanisms. This could improve the balance between retaining relevant deformation signals and excluding non-landslide-related motion.

Standard InSAR filtering approaches—such as sensitivity index, detectability power, and geometric constraints—are effective in ensuring signal quality, but they are not sufficient to guarantee that the detected deformation is related to landslide processes. These filters should therefore be complemented with geomorphological constraints, as high-quality signals can still represent non-landslide deformation, particularly in urban or low-gradient areas.

The findings of this study indicate that InSAR-derived deformation should be used to complement existing landslide inventories rather than replace them. Its value lies in identifying potentially active areas and enriching spatial information, but only when integrated within a framework that preserves the geomorphological controls of landslides.

Bibliography

Ado, M., Amitab, K., Maji, A. K., Jasińska, E., Gono, R., Leonowicz, Z., & Jasiński, M. (2022). Landslide Susceptibility Mapping Using Machine Learning: A Literature survey. *Remote Sensing*, *14*(13), 3029. https://doi.org/10.3390/rs14133029

Agboola, G., Beni, L. H., Elbayoumi, T., & Thompson, G. (2024). Optimizing landslide susceptibility mapping using machine learning and geospatial techniques. *Ecological Informatics*, *81*, 102583. https://doi.org/10.1016/j.ecoinf.2024.102583

Bacino Distrettuale, A. M. (2025, March). Autorità di Bacino Distrettuale dellAppennino Meridionale. https://www.distrettoappenninomeridionale.it/piano-stralcio-assetto-idrogeologico-rischio-da-frana/uom-regionale-campania-nord-occidentale-uom-sarno-ex-adb-reg-campania-centrale/

Bell, R., Glade, T., Granica, K., Heiss, G., Leopold, P., Petschko, H., Pomaroli, G., Proske, H., & Schweigl, J. (2013, January). *Landslide Susceptibility Maps for Spatial Planning in Lower Austria*. https://doi.org/10.1007/978-3-642-31325-7\{_}60

Berrar. (2019). Cross-validation.

Bogaard, T. A., & Greco, R. (2015). Landslide hydrology: from hydrology to pore pressure. *Wiley Interdisciplinary Reviews Water*, *3*(3), 439–459. https://doi.org/10.1002/wat2.1126

Carrara, A. (1983). Multivariate models for landslide hazard evaluation. *Mathematical Geology*, *15*(3), 403–426. https://doi.org/10.1007/bf01031290

Cascini, L. (2008). Applicability of landslide susceptibility and hazard zoning at different scales. *Engineering Geology*, *102*(3-4), 164–177. https://doi.org/10.1016/j.enggeo.2008.03.016

Catani, F., Lagomarsino, D., Segoni, S., & Tofani, V. (2013). Landslide susceptibility estimation by random forests technique: sensitivity and scaling issues. *Natural hazards and earth system sciences*, *13*(11), 2815–2831. https://doi.org/10.5194/nhess-13-2815-2013

Centro Funzionale Multirischi di Protezione Civile Regione Campania. (n.d.). https://centrofunzionale.regione.campania.it/home#/pages/sensori/archivio-pluviometrici

Chacón, J., Irigaray, C., Fernández, T., & Hamdouni, R. E. (2006). Engineering geology maps: landslides and geographical information systems. *Bulletin of Engineering Geology and the Environment*, *65*(4), 341–411. https://doi.org/10.1007/s10064-006-0064-z

Chang, L., Dollevoet, R. P. B. J., & Hanssen, R. F. (2018). Monitoring Line-Infrastructure with Multisensor SAR Interferometry: Products and performance assessment metrics. *IEEE Journal of Selected Topics in Applied Earth Observations and Remote Sensing*, *11*(5), 1593–1605. https://doi.org/10.1109/jstars.2018.2803074

Chen, L., Ma, P., Yu, C., Zheng, Y., Zhu, Q., & Ding, Y. (2023). Landslide susceptibility assessment in multiple urban slope settings with a landslide inventory augmented by InSAR techniques. *Engineering Geology*, *327*, 107342. https://doi.org/10.1016/j.enggeo.2023.107342

Chung, C.-J. F., & Fabbri, A. G. (1999). Probabilistic Prediction Models for Landslide Hazard Mapping. *Photogrammetric Engineering & Remote Sensing*, *65*(12), 1389–1399. https://doi.org/10.1002/9780470012659.ch4

Cruden, D. M. (1991). A simple definition of a landslide. *Bulletin of Engineering Geology and the Environment*, *43*(1), 27–29. https://doi.org/10.1007/bf02590167

Danesi, S., Carlino, S., & Pino, N. A. (2025). Tracking the November 26, 2022, Casamicciola debris flow through seismic signals (Ischia, southern Italy). *Landslides*, *23*(3), 837–850. https://doi.org/10.1007/s10346-025-02626-4

De Vita, P., & Nappi, M. (2013, January). *Regional Distribution of Ash-Fall Pyroclastic Soils for Landslide Susceptibility Assessment*. https://doi.org/10.1007/978-3-642-31310-3\{_}15

De Winter, J. C. F., Gosling, S. D., & Potter, J. (2016). Comparing the Pearson and Spearman correlation coefficients across distributions and sample sizes: A tutorial using simulations and empirical data. *Psychological Methods*, *21*(3), 273–290. https://doi.org/10.1037/met0000079

Devkota, K. C., Regmi, A. D., Pourghasemi, H. R., Yoshida, K., Pradhan, B., Ryu, I. C., Dhital, M. R., & Althuwaynee, O. F. (2012). Landslide susceptibility mapping using certainty factor, index of entropy and logistic regression models in GIS and their comparison at Mugling–Narayanghat

road section in Nepal Himalaya. *Natural Hazards*, *65*(1), 135–165. https://doi.org/10.1007/s11069-012-0347-6

Dou, J., Yunus, A. P., Bui, D. T., Sahana, M., Chen, C.-W., Zhu, Z., Wang, W., & Pham, B. T. (2019). Evaluating GIS-Based multiple statistical models and data mining for earthquake and Rainfall-Induced Landslide susceptibility using the LIDAR DEM. *Remote Sensing*, *11*(6), 638. https://doi.org/10.3390/rs11060638

Emberson, R., Kirschbaum, D. B., Amatya, P., Tanyas, H., & Marc, O. (2022). Insights from the topographic characteristics of a large global catalog of rainfall-induced landslide event inventories. *Natural hazards and earth system sciences*, *22*(3), 1129–1149. https://doi.org/10.5194/nhess-22-1129-2022

Evans, S., Mugnozza, G., Strom, A., Hermanns, R., Ischuk, A., & Vinnichenkos, S. (2006). Landslides from massive rock slope failure and associated phenomena. *Landslides*, *49*, 3–52.

Fell, R., Corominas, J., Bonnard, C., Cascini, L., Leroi, E., & Savage, W. Z. (2008). Guidelines for landslide susceptibility, hazard and risk zoning for land use planning. *Engineering Geology*, *102*(3-4), 85–98. https://doi.org/10.1016/j.enggeo.2008.03.022

Feng, X., Du, J., Chai, B., & Bogaard, T. (2025). Combining landslide inventories with deformation time series: A methodology. *n/a*. https://doi.org/10.5194/egusphere-egu25-8480

Ferretti, A., Prati, C., & Rocca, F. (2001). Permanent scatterers in SAR interferometry. *IEEE Transactions on Geoscience and Remote Sensing*, *39*(1), 8–20. https://doi.org/10.1109/36.898661

Fidan, S., Tanyaş, H., Akbaş, A., Lombardo, L., Petley, D. N., & Görüm, T. (2024). Understanding fatal landslides at global scales: a summary of topographic, climatic, and anthropogenic perspectives. *Natural Hazards*, *120*(7), 6437–6455. https://doi.org/10.1007/s11069-024-06487-3

Fredlund, D. G., & Rahardjo, H. (1993, August). *Soil mechanics for unsaturated soils*. https://doi.org/10.1002/9780470172759

Froude, M. J., & Petley, D. N. (2018). Global fatal landslide occurrence from 2004 to 2016. *Natural hazards and earth system sciences*, *18*(8), 2161–2181. https://doi.org/10.5194/nhess-18-2161-2018

Geertsema, M., Highland, L., & Vaugeouis, L. (2008, November). *Environmental Impact of Landslides*. https://doi.org/10.1007/978-3-540-69970-5\{_}31

Geertsema, M., & Pojar, J. J. (2006). Influence of landslides on biophysical diversity — A perspective from British Columbia. *Geomorphology*, *89*(1-2), 55–69. https://doi.org/10.1016/j.geomorph.2006.07.019

Guzzetti, F. (2000). Landslide fatalities and the evaluation of landslide risk in Italy. *Engineering Geology*, *58*(2), 89–107. https://doi.org/10.1016/s0013-7952(00)00047-8

Guzzetti, F., Mondini, A. C., Cardinali, M., Fiorucci, F., Santangelo, M., & Chang, K.-T. (2012). Landslide inventory maps: New tools for an old problem. *Earth-Science Reviews*, *112*(1-2), 42–66. https://doi.org/10.1016/j.earscirev.2012.02.001

Hanssen, R. F. (2001, April). *Radar Interferometry: Data interpretation and error analysis*. https://doi.org/10.1007/0-306-47633-9

Haque, U., Blum, P., Da Silva, P. F., Andersen, P., Pilz, J., Chalov, S. R., Malet, J.-P., Auflič, M. J., Andres, N., Poyiadji, E., Lamas, P. C., Zhang, W., Peshevski, I., Pétursson, H. G., Kurt, T., Dobrev, N., García-Davalillo, J. C., Halkia, M., Ferri, S., … Keellings, D. (2016). Fatal landslides in Europe. *Landslides*, *13*(6), 1545–1554. https://doi.org/10.1007/s10346-016-0689-3

Haque, U., Da Silva, P. F., Devoli, G., Pilz, J., Zhao, B., Khaloua, A., Wilopo, W., Andersen, P., Lu, P., Lee, J., Yamamoto, T., Keellings, D., Wu, J.-H., & Glass, G. E. (2019). The human cost of global warming: Deadly landslides and their triggers (1995–2014). *The Science of The Total Environment*, *682*, 673–684. https://doi.org/10.1016/j.scitotenv.2019.03.415

Harp, E. L., Keefer, D. K., Sato, H. P., & Yagi, H. (2011). Landslide inventories: The essential part of seismic landslide hazard analyses [The next generation of research on earthquake-induced landslides]. *Engineering Geology*, *122*(1), 9–21. https://doi.org/https://doi.org/10.1016/j.enggeo.2010.06.013

Hong, H., Miao, Y., Liu, J., & Zhu, A.-X. (2019). Exploring the effects of the design and quantity of absence data on the performance of random forest-based landslide susceptibility mapping. *CATENA*, *176*, 45–64. https://doi.org/10.1016/j.catena.2018.12.035

Huang, F., Li, R., Catani, F., Zhou, X., Zeng, Z., & Huang, J. (2024). Uncertainties in landslide susceptibility prediction: Influence rule of different levels of errors in landslide spatial position. *Journal*

of Rock Mechanics and Geotechnical Engineering, *16*(10), 4177–4191. https://doi.org/10.1016/j.jrmge.2024.02.001

Huang, F., Yan, J., Fan, X., Yao, C., Huang, J., Chen, W., & Hong, H. (2021). Uncertainty pattern in landslide susceptibility prediction modelling: Effects of different landslide boundaries and spatial shape expressions. *Geoscience Frontiers*, *13*(2), 101317. https://doi.org/10.1016/j.gsf.2021.101317

Hungr, O., Leroueil, S., & Picarelli, L. (2013). The Varnes classification of landslide types, an update. *Landslides*, *11*(2), 167–194. https://doi.org/10.1007/s10346-013-0436-y

Hussin, H. Y., Zumpano, V., Reichenbach, P., Sterlacchini, S., Micu, M., Van Westen, C., & Bălteanu, D. (2015). Different landslide sampling strategies in a grid-based bi-variate statistical susceptibility model. *Geomorphology*, *253*, 508–523. https://doi.org/10.1016/j.geomorph.2015.10.030

Intrieri, E., Raspini, F., Fumagalli, A., Lu, P., Del Conte, S., Farina, P., Allievi, J., Ferretti, A., & Casagli, N. (2017). The Maoxian landslide as seen from space: detecting precursors of failure with Sentinel-1 data. *Landslides*, *15*(1), 123–133. https://doi.org/10.1007/s10346-017-0915-7

Iverson, R. M. (2000). Landslide triggering by rain infiltration. *Water Resources Research*, *36*(7), 1897–1910. https://doi.org/10.1029/2000wr900090

J., H. M. (1984). Strategies for classification of landslides. *Slope Instability*, 1–25. https://cir.nii.ac.jp/crid/1572261549374959872

Kampes, B. (2006, August). *Radar Interferometry: persistent scatterer technique*. https://doi.org/10.1007/978-1-4020-4723-7

Kang, Y., Lu, Z., Zhao, C., Xu, Y., Kim, J.-W., & Gallegos, A. J. (2021). InSAR monitoring of creeping landslides in mountainous regions: A case study in Eldorado National Forest, California. *Remote Sensing of Environment*, *258*, 112400. https://doi.org/10.1016/j.rse.2021.112400

Kilburn, C. R., & Petley, D. N. (2003). Forecasting giant, catastrophic slope collapse: lessons from Vajont, Northern Italy. *Geomorphology*, *54*(1-2), 21–32. https://doi.org/10.1016/s0169-555x(03)00052-7

Kirschbaum, D., Stanley, T., & Zhou, Y. (2015). Spatial and temporal analysis of a global landslide catalog. *Geomorphology*, *249*, 4–15. https://doi.org/10.1016/j.geomorph.2015.03.016

Korup, O. (2005). Large landslides and their effect on sediment flux in South Westland, New Zealand. *Earth Surface Processes and Landforms*, *30*(3), 305–323. https://doi.org/10.1002/esp.1143

Lazarte, C. A., Robinson, H. D., Gómez, J., Baxter, A., Cadden, A., & Berg, R. R. (2015). Soil Nail Walls Reference Manual. *Soil Nail Walls Reference Manual*. https://trid.trb.org/view/1352016

Li, B. V., Jenkins, C. N., & Xu, W. (2022). Strategic protection of landslide vulnerable mountains for biodiversity conservation under land-cover and climate change impacts. *Proceedings of the National Academy of Sciences*, *119*(2). https://doi.org/10.1073/pnas.2113416118

Lombardo, L., & Mai, P. M. (2018). Presenting logistic regression-based landslide susceptibility results. *Engineering Geology*, *244*, 14–24. https://doi.org/10.1016/j.enggeo.2018.07.019

Maddalwar, S., Kumar, T., Tijare, G., Agashe, A., Kotangale, P., Sawarkar, A., & Singh, L. (2024). A global perspective on a bioengineering approach to landslide mitigation using bamboo diversity. *Advances in Bamboo Science*, *8*, 100093. https://doi.org/10.1016/j.bamboo.2024.100093

Massonnet, D., Rossi, M., Carmona, C., Adragna, F., Peltzer, G., Feigl, K., & Rabaute, T. (1993). The displacement field of the Landers earthquake mapped by radar interferometry. *Nature*, *364*(6433), 138–142. https://doi.org/10.1038/364138a0

Merghadi, A., Yunus, A. P., Dou, J., Whiteley, J., ThaiPham, B., Bui, D. T., Avtar, R., & Abderrahmane, B. (2020). Machine learning methods for landslide susceptibility studies: A comparative overview of algorithm performance. *Earth-Science Reviews*, *207*, 103225. https://doi.org/10.1016/j.earscirev.2020.103225

Montgomery, D. R., & Dietrich, W. E. (1994). A physically based model for the topographic control on shallow landsliding. *Water Resources Research*, *30*(4), 1153–1171. https://doi.org/10.1029/93wr02979

Notti, D., Herrera, G., Bianchini, S., Meisina, C., García-Davalillo, J. C., & Zucca, F. (2014). A methodology for improving landslide PSI data analysis. *International Journal of Remote Sensing*, *35*(6), 2186–2214. https://doi.org/10.1080/01431161.2014.889864

Nugraha, D. H., Wilopo, W., & Fathani, T. F. (2026). Landslide Susceptibility Mapping using the Weight of Evidence Model: a case study on a tropical volcanic region. *Journal of Multidisciplinary Applied Natural Science*. https://doi.org/10.47352/jmans.2774-3047.350

Petley, D. (2012). Global patterns of loss of life from landslides. *Geology*, *40*(10), 927–930. https://doi.org/10.1130/g33217.1

Protection, I. C. (2026, January). Niscemi Landslide. https://emergenze.protezionecivile.gov.it/en/meteo-hydro/niscemi-landslide-2026

Reichenbach, P., Rossi, M., Malamud, B. D., Mihir, M., & Guzzetti, F. (2018). A review of statistically-based landslide susceptibility models. *Earth-Science Reviews*, *180*, 60–91. https://doi.org/10.1016/j.earscirev.2018.03.001

Rigon, R., Bertoldi, G., & Over, T. M. (2006). GEOtop: A Distributed Hydrological Model with Coupled Water and Energy Budgets. *Journal of Hydrometeorology*, *7*(3), 371–388. https://doi.org/10.1175/jhm497.1

Sansivero, F. (n.d.). Le Reti Geodetiche di Ischia. https://www.ov.ingv.it/index.php/monitoraggio-geodetico/ischia-mon-geodetico

Santangelo, M., Marchesini, I., Bucci, F., Cardinali, M., Fiorucci, F., & Guzzetti, F. (2015). An approach to reduce mapping errors in the production of landslide inventory maps. *Natural hazards and earth system sciences*, *15*(9), 2111–2126. https://doi.org/10.5194/nhess-15-2111-2015

Schuster, R. L., & Highland, L. M. (n.d.). *Impact of Landslides and Innovative Landslide-Mitigation Measures on the Natural Environment* (tech. rep.). Geologic Hazards Team, U.S. Geological Survey. https://pubs.usgs.gov/op/HongKongJuly/HongKongJuly21.pdf

Schuster, R. L., & Highland, L. M. (2007). Overview of the effects of mass wasting on the natural environment. *Environmental and Engineering Geoscience*, *13*(1), 25–44. https://doi.org/10.2113/gseegeosci.13.1.25

Sepúlveda, S. A., & Petley, D. N. (2015). Regional trends and controlling factors of fatal landslides in Latin America and the Caribbean. *Natural hazards and earth system sciences*, *15*(8), 1821–1833. https://doi.org/10.5194/nhess-15-1821-2015

Steger, S., Brenning, A., Bell, R., & Glade, T. (2017). The influence of systematically incomplete shallow landslide inventories on statistical susceptibility models and suggestions for improvements. *Landslides*, *14*(5), 1767–1781. https://doi.org/10.1007/s10346-017-0820-0

Steger, S., Brenning, A., Bell, R., & Glade, T. (2016). The propagation of inventory-based positional errors into statistical landslide susceptibility models. *Natural hazards and earth system sciences*, *16*(12), 2729–2745. https://doi.org/10.5194/nhess-16-2729-2016

Stock, G., Luco, N., Collins, B., Harp, E., Paola, R., & Frankel, K. (2011). Quantitative rock-fall hazard and risk assessment for yosemite valley, california. *AGU Fall Meeting Abstracts*, 04–.

Stokes, A., Norris, J. E., Van Beek, L. P. H., Bogaard, T., Cammeraat, E., Mickovski, S. B., Jenner, A., Di Iorio, A., & Fourcaud, T. (2008, January). *How Vegetation Reinforces Soil on Slopes*. https://doi.org/10.1007/978-1-4020-6676-4\{_}4

Tarquini, S., Isola, I., Favalli, M., Battistini, A., & Dotta, G. (2022, January). TINITALY, a digital elevation model of Italy with a 10 meters cell size, version 1.1. https://doi.org/10.13127/tinitaly/1.1

Teunissen, P. J. (2024, June). *Testing theory*. https://doi.org/10.59490/tb.96

U.S. Department of Agriculture, Natural Resources Conservation Service. (2022). *Basic soils alaska curriculum*. U.S. Department of Agriculture, Natural Resources Conservation Service. https://www.nrcs.usda.gov/sites/default/files/2022-10/Basic_Soils_AK_Curriculm%20-%20UPDATED.pdf

Van Natijne, A., Bogaard, T., Van Leijen, F., Hanssen, R., & Lindenbergh, R. (2022). World-wide InSAR sensitivity index for landslide deformation tracking. *International Journal of Applied Earth Observation and Geoinformation*, *111*, 102829. https://doi.org/10.1016/j.jag.2022.102829

Van Westen, C. J., Castellanos, E., & Kuriakose, S. L. (2008). Spatial data for landslide susceptibility, hazard, and vulnerability assessment: An overview. *Engineering Geology*, *102*(3-4), 112–131. https://doi.org/10.1016/j.enggeo.2008.03.010

Varnes, D. J. (1957). *Landslides and Engineering Practice*. Idaho Department Highways. https://onlinepubs.trb.org/Onlinepubs/sr/sr29/sr29.pdf

Vinueza, A. U., Handwerger, A. L., Bakker, M., & Bogaard, T. (2022). A new method to detect changes in displacement rates of slow-moving landslides using InSAR time series. *Landslides*, *19*(9), 2233–2247. https://doi.org/10.1007/s10346-022-01913-8

Wei, Y., Qiu, H., Liu, Z., Huangfu, W., Zhu, Y., Liu, Y., Yang, D., & Kamp, U. (2024). Refined and dynamic susceptibility assessment of landslides using InSAR and machine learning models. *Geoscience Frontiers*, *15*(6), 101890. https://doi.org/10.1016/j.gsf.2024.101890

Woodard, J. B., & Mirus, B. B. (2025). Overcoming the data limitations in landslide susceptibility modeling. *Science Advances*, *11*(8), eadt1541. https://doi.org/10.1126/sciadv.adt1541

Zebker, H., & Villasenor, J. (1992). Decorrelation in interferometric radar echoes. *IEEE Transactions on Geoscience and Remote Sensing*, *30*(5), 950–959. https://doi.org/10.1109/36.175330

Zhou, X., Wen, H., Zhang, Y., Xu, J., & Zhang, W. (2021). Landslide susceptibility mapping using hybrid random forest with GeoDetector and RFE for factor optimization. *Geoscience Frontiers*, *12*(5), 101211. https://doi.org/10.1016/j.gsf.2021.101211

Zhu, Z., Gan, S., Yuan, X., & Zhang, J. (2022). Landslide Susceptibility Mapping with Integrated SBAS-InSAR Technique: A Case Study of Dongchuan District, Yunnan (China). *Sensors*, *22*(15), 5587. https://doi.org/10.3390/s22155587

A

Static maps of Ischia

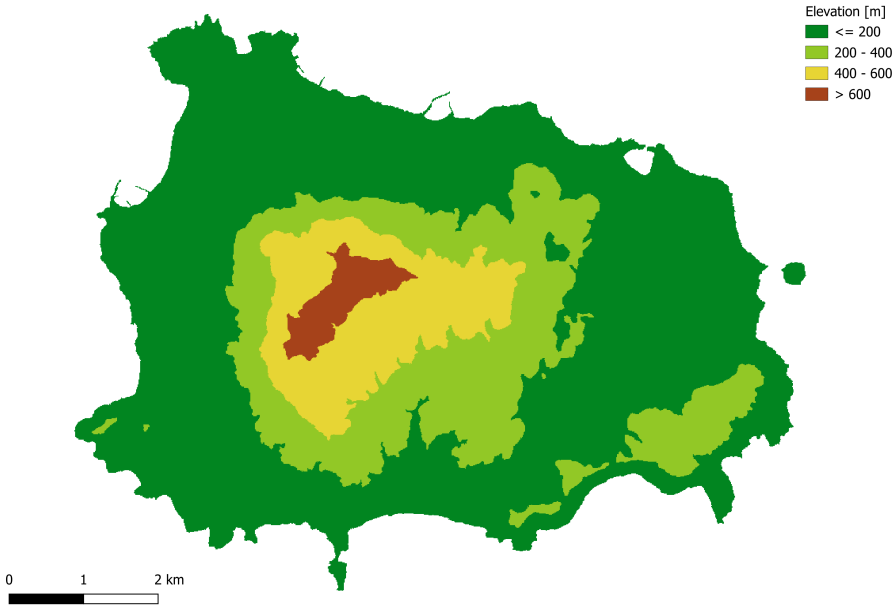

Figure A.1: Elevation map

Figure A.2: Land cover map

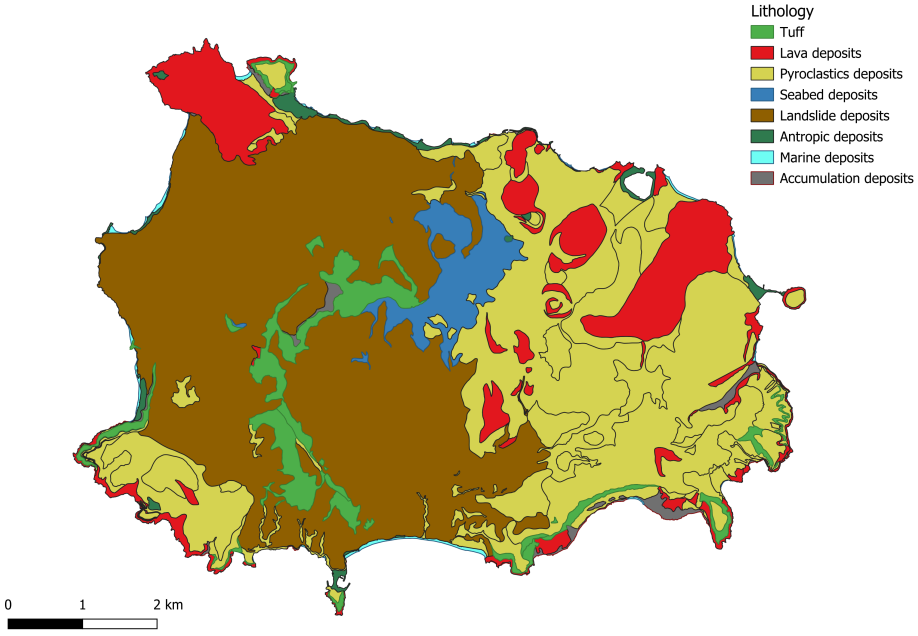

Figure A.3: Lithology map

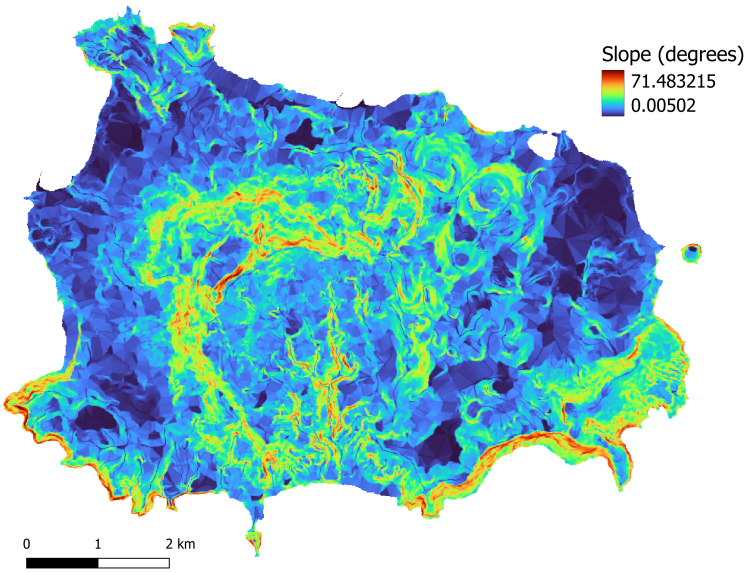

Figure A.4: Slope map